DESIGN AND DEVELOPMENT OF LOW HEAD SMALL HYDRO TURBINES IN PAKISTAN

AJAZ BASHIR JANJUA
04-UET/PhD-ME-07
February 2013

Supervisor

Prof. Dr. M.Shahid Khalil

Department of Mechanical Engineering

Faculty of Mechanical and Aeronautical Engineering

University of Engineering & Technology, Taxila, Pakistan

ABSTRACT

Utilization of hydro-power as renewable energy source is of great concern now-a-days. Hydro-power energy is abundantly available in different forms. Hydropower energy can be achieved from potential hydro sites with sufficient water discharge and pressure heads. For this purpose, selected types of hydro turbines can be designed and developed depending upon the site locations.

Low head small hydro turbines are preferably used on run-of-river to produce the hydro-electric power. Research work on low head turbines can lead to achieve the maximum output and more efficiency using the latest computational techniques.

In this dissertation, research work is presented on the blade profile optimization of the complex geometry to enhance the power output of the low head Kaplan turbine for the given head of water and different discharge conditions. Before application of the computational fluid dynamics, thorough study and development work on the blade profile have been carried out.

As-built data of the sample blade was worked out at shop floor using the well calibrated measuring instruments. To ensure better quality of the work, coordinate points taken were rechecked by the qualified QA personnel.

Coordinate points data was imported in the Pro-E / Creo software for the preparation of 3D CAD model of the blade. Finally, the blade CAD model was prepared after several attempts due to the complex geometry of profile. Assembly of the developed blade model was carried out with the shaft and hub for the purpose of CFD analysis to validate the model.

Results obtained were validated with the experimental / operational data. After successful validation, four different blade profiles have been developed.

Research results show improvement in the power output of the turbine with 5.43%. Future recommendations were also suggested to pave the way of further improvement in this area of specialization.

Keywords:

Low Head, Kaplan Turbine, Runner Blade, CFD, Optimization, Hydropower, Run-of-River

DECLARATION

I certify that research work titled "*Design and Development of Low-Head Small Hydro Turbines in Pakistan"* is my own work. The work has not, in whole or in part, been presented elsewhere for assessment. Where material has been used from other sources it has been properly acknowledged / referred.

Ajaz Bashir Janjua

04-UET/PhD-ME-07

ACKNOWLEDGEMENTS

Thanks **Al-Mighty-Allah** who enable me to do research on Kaplan Turbine. I am thankful to all those people who helped and supported me during this research and made it possible.

My deep gratitude goes to my PhD supervisor, Professor Dr. M.Shahid Khalil for his supervision, continuous support, encouragement, research approach and expertise in research work. The efforts and valuable guidance of Prof. Dr. M. Shahid Khalil made it possible for me not only to serve the purpose but also to enhance my research skills as well. I am very grateful for his inspiration and guidance throughout the research work.

My deep gratitude also goes to my Research Committee members, comprising of Dr. Brig. Atiq-u-Rehman (Late), Dr. Khalid Akhtar, and Dr. Mahmood Anwar, for their support, guidance and encouragement during the research work.

I specially owe my deep gratitude to Dr. Fahad Butt, Mr. Muhammad Saeed, Dr. Tariq Manzoor, Mr. Atta-ur-Rehman, Syed Rasheed Hoda for their support, technical discussions and sharing their knowledge & expertise specifically in the field of CFD analysis/simulations throughout the research work.

I specially owe my deep gratitude to Dr. M. Ashraf Butt, Managing Director (HMC) for his kind hearted support and encouragement, enabling me to complete this task.

My deep gratitude also goes to Hafiz Muhammad Jamil R.E Nandi-pur HPP and his team for supporting and providing all the help at site.

I would also like to thank of all faculty members and officials of Mechanical Engineering Department, Dean, Chairman, my colleagues, my parents and family who always helped me and prayed for my success. I always remember their support and contributions for the completion of this research work.

Engr. Ajaz Bashir Janjua

DEDICATION

Dedicated to my dearest parents,

adoring wife & children and family

members whose prays, love, sacrifices

and encouragement is boundless.

TABLE OF CONTENTS

LIST OF FIGURES

LIST OF TABLES

NOMENCLATURE

P	Power
ρ	density of water
g	gravitational acceleration
h	Head of water
Q	Discharge
η	Hydraulic efficiency
CFD	Computational Fluid Dynamics
SPD	Survey of Pakistan Datum
CAD	Computer Aided Design
MW	Mega Watt
KW	Kilo Watt
SEM	Scanning Electron Microscopy
XRD	X-ray Diffraction
AOD	Argon Oxygen Decarburization
VOD	Vacuum Oxygen Decarburization
FeSi	Ferro Silicon
MnSi	Manganese Silicon
FeCr	Ferro Chromium
FeTi	Ferro Titanium
HRC	Rockwell Hardness
ASTM	American Society for Testing and Materials

CHAPTER 1

1 INTRODUCTION

Use of renewable energy is very demanding over the last few years due to environmental issues. Serious changes in the climate are occurring due to the high emissions of greenhouse gases. Widely used renewable energy sources include wind, solar and water energy. Use of hydropower energy can solve the problem of energy crisis in the world.

Hydropower energy has been used for many years, for instance, to grinding grain. Simple water wheels were used for this purpose. Over the years water turbines have been developed and become more and more advanced. Now-a-days hydropower is the most important energy source available. Hydropower is contributing around 20% of energy world-wide.

1.1 Motivation

Development of the latest technological techniques of hydro-mechanical equipments especially water turbines has been of general interest to the scientific and engineering communities for many years. Many researchers have used different techniques for the development of hydro turbines. Most of the work has been done using latest CFD techniques.

1.2 Overview

Hydro turbines are the fundamental elements in hydro-mechanical equipments and play a significant role for power production. In this dissertation, design aspects for hydro turbines, fabrication of a Kaplan turbine runner blade, and optimization of Kaplan turbine runner blade using CFD are discussed.

1.2.1 Hydro-power as Renewable Energy Resource

Hydropower is currently the largest and most easily accessible power source in the renewable energy sources to generate electricity due to its high energy

density [1].

The hydroelectric power plant has to be installed with adequate turbine type in order to achieve the maximum output and higher efficiency. There are several different kinds of water turbines and can be divided into impulse and reaction turbines. An impulse turbine is where the water pressure is transformed into kinetic energy before the water reaches the runner of the turbine. The energy hits the runner in a form of a high-speed jet. A turbine, where the water pressure applies a force on the face of the runner blade is called a reaction turbine. Three types of turbines i-e 1) Pelton, 2) Francis and 3) Kaplan are usually utilized in the modern field of hydropower:

Pelton turbine is classified as impulse turbine. It is consisted of a wheel having number of buckets fixed on the wheel periphery on which water impinges to rotate the wheel.

Francis turbine is classified as reaction turbine. It has fixed blades with adjustable wicket gates. These are generally of vertical axis type.

Kaplan turbine is a reaction turbine. It is preferably used at sites having large amount of water at low heads. Runner of the Kaplan turbine resembles with the shape of propeller of a ship. Kaplan turbines are also called propeller turbine. These turbines are applicable for a head range from 2m to 40m.

1.2.1.1 Hydropower Theory

Energy from falling water and from run-of-river can be harnessed to obtain electrical power. Theoretical energy from a site depends on the flow of the water and the height of the water fall at the site. In order to estimate the hydropower potential from a site, it is important that the head and the flow of water over a period of time be measured.

Power available is proportional to the product of head of water and discharge through the turbine [2]. The general formula for any hydro system's power output is as given in Equation 1.1:

$$P = \rho g h Q \eta \quad (1.1)$$

Where, P is the mechanical power produced at the turbine shaft (Watts), ρ is the density of water (kg/m^3), g is the acceleration due to gravity (m/s^2), h is the effective pressure head of water across the turbine (m), Q is the discharge through the turbine (m^3/s) and η is the hydraulic efficiency of the turbine. Annual energy produced in kWh year is expressed in Equation 1.2;

$$\text{Annual energy (kWh/year)} = P\,(KW) \times CP \times 24\ hrs \times 365\ days \quad (1.2)$$

Where CP is the capacity factor, which indicates how long the turbine unit will be in operation.

1.2.1.2 Hydro-power Classification

Small hydropower based on the installed capacity have been classified inconsistently throughout the hydro-power literature [3]. Small hydro-power can be classified as less than 5MW and greater than 1 MW [4].

Micro hydropower is generally defined as having power less than or equal to 100 kW [2], [5]. Based on the current literature, hydro-power classification can be set as shown in Table 1.1

Table 1.1: **Classification of small scale hydropower**

S. No	Type	Unit Capacity
1	Micro-Hydro	Up to 100 kW
2	Mini-Hydro	101 to 1000 kW
3	Small-Hydro	1001 to 5000 kW

1.2.2 Hydro-power in Pakistan

Pakistan is enriching in hydro-power potential to be capable of generating around 50,000 MW [62]. But this potential has not contributed any significant role in producing the hydro-electrical energy in the country. Hydro power generation is the only solution to control the energy crisis. The industrial development of any country is mostly based on the utilization of natural power recourses. Theses power recourses not only fulfil the electricity requirement of the country but can play an important role in the industrial and technological development of the country.

In Pakistan, mineral oil and natural gas occupy an important place. From these resources, 75% electricity requirements are fulfilled. Hydro-power resources contribute approximately 18% electricity, whereas by coal 6% and about 1% electricity from other resources.

The small hydro is by far the best option available for Pakistan due to the presence of many rivers, the environmental and societal benefits. Present installed capacity of hydro-power about 6464 MW [6] is as shown in Figure 1.1

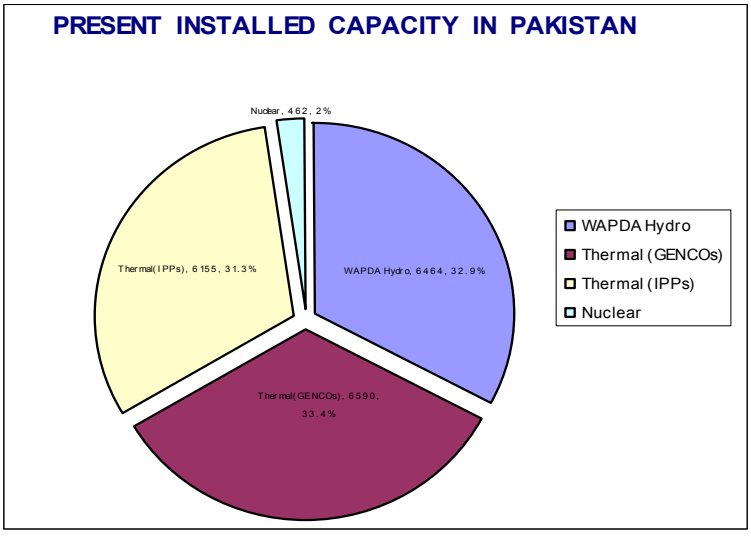

Figure 1.1: Installed capacity of hydro-power in Pakistan

1.3 Research Objectives

Due to recent crises of electricity in the country, it is utmost need for the utilization of renewable energy resources abundantly available like hydro-power. To overcome this problem of electricity shortage, hydro-power turbines can be used. Since every hydro site have different site conditions, so design and selection of the proper turbine type and size becomes more important.

In this case, it is vital to adopt indigenous design and development of hydro-power components. Hydro turbines are the most important part of hydro-power plant. In this research, development of turbines has been focused, mainly of low head turbines. The reason is that small low-head schemes can easily be executed on the run-off-rivers and canals. This research proposes the basic design and development of a Kaplan turbine blade profile using the computational fluid dynamics (CFD) approach. Optimization of the blade of Kaplan turbine runner blade have been carried out by developing geometrical changes on blade profile and compared with the actual site data for validation purpose.

Main focus in this research is on the development of 3D CAD model based on actual as-built data of blade. Other activities include the preparation of complex profile surfaces / outlines, static analysis of the blade for structural stability, mesh independence study for CFD, computational fluid dynamic analysis, validation of the results with experimental data, development of different modified models (case-B, case-C, case-D and case-E in this study) with changed profiles for optimization purpose, CFD analysis on the modified models and finally results comparison with experimental data for the improvement in power output. Utilization of CFD is not only a cost effective tool but also ensures design stabilities.

1.4 Research Outline and Methodology

Methodology of the work has been elaborated in detail chapter-wise. Chapter-1 outlines the introduction about the history of hydro-power development. In our

study, design and development of the low head hydro-power turbines have been covered and discussed.

Chapter-2 indicates the literature survey / review carried out for the development of hydro-power not only through conventional methods but also utilizing the computational techniques i.e. CFD analysis.

Chapter-3 illustrates the design procedure of the Kaplan turbine blades development. Coordinate point as-built data of the blade profile have been taken with precise calibrated tools. Final data imported in Pro-E/ Creo for the development of 3D-CAD model and preparation of CAD drawings are discussed in the chapter.

Chapter-4 illustrates the manufacturing procedure of the runner blade in detail.

In chapter-5 behaviour of static stress analysis for the structural stability is being illustrated.

Chapter-6 illustrates utilization of the computational fluid dynamics (CFD) on the runner blade profiles. Preparation of the blade models is being carried based on the actual as-built blade profile data. Complex surface profile being the main development issue has been successfully prepared for the purpose of onward analysis. Mesh independence study have been carried out for proper meshing. Validation of the CFD results has been discussed in detail. Further CFD work has been discussed for the optimization of different blade profiles.

Chapter-7 summarises the main conclusions of this work and highlighted recommendations for further work.

CHAPTER 2

2 LITERATURE REVIEW

2.1 Introduction

To discuss general historical background on the hydro turbines, we begin with review on the design and development of different types of hydro turbines, their types, their uses and research work carried out on their development from different technical aspects. This is followed by the design aspects of turbines.

Zhou, L, et al. [7] studied that dynamic stresses in blades are related to hydraulic instability as shown by the flow calculations and measured stresses. Studies were also carried out for calculating the dynamic stresses caused by the unsteady hydraulic loadings. Thereafter dynamic interaction problem in blades was analyzed. It was done from solution of 3D unsteady flow through its flow passage.

Unsteady RANS equations were solved for modelling the flow within the complete flow path of the turbine and so the hydraulic forces were used as the boundary condition. Dynamic stresses in the blade were found low under the optimum operating conditions and were high under low-output conditions.

It indicated that prediction of dynamic stresses is possible during design stage. However it is recommended to check the safety factor while designing for 100 percent output with lower head and for 50 percent output with the highest head.

2.2 Computational Fluid Dynamics (CFD)

Computational Fluid Dynamics (CFD) has been used extensively in the field of research and development of the components used in the industrial setup. It is mostly utilized in the area of turbo-machinery including hydro turbines.

Swiderski J., et al. [8] carried out research worked on the universal design methodology for water turbines. Interactive geometry editor was coupled through data files using the 3D viscous flow analysis software. Researchers presented the general structure of the design algorithm as well as example of the design optimization. It illustrated that authors are using it for design purposes in the small hydropower field assuming the trustworthiness of the CFD results.

Bennett K., and Swiderski, J. [9] worked for the remedy of severe blade cavitations and hub seal failure at Elliott Fall small-hydro generating station.

Replacement of the pumps with new small-hydro turbines was considered in the study. As a solution, existing stays vanes, hub and blades were replaced with a custom runner and distributor. These were designed and developed using computational fluid dynamics (CFD) techniques. Their study illustrated the original design work of the power plant, the problems encountered, the solutions adopted, and the repair/upgrade results. It indicates the utilization of CFD for the custom design of small-hydro turbines is not only appropriate but cost-effective tool.

Grekula, M., and Bark, G.O. [10] carried work on the cavitations present in a Kaplan model turbine to identify mechanisms which are the basic cause for promoting the erosive cavitations. For this purpose, high-speed video filming, and visual observations were made and as a result periodic pattern was observed. Main feature of that pattern was that cavitating vortex was bent towards blade surface and transformed into cloud formations. The clouds were found collapsing each other which can be suggested an erosive process.

This collapse was found on the periphery of the blade sustaining the damages. It was also found that cloud formations appeared in bands with periodicity corresponding to the spacing between the guide vanes.

The cavities seem to be of mainly sheet or travelling bubble type at the blade root depending upon the running condition. Also few facts show the contribution of vortex motion.

Laura A. et al. [11] carry on research by using CFD to display and quantify the areas of elevated shear stress in turbine operating at different flow conditions.CFD results were compared to field test data at the same flow conditions.

For the development of design concepts for improving the compatibility of hydro turbines with the environment, U.S. Department of Energy initiated the program to contribute improvement in the fish-friendliness of turbine designs by providing biological design criteria to guide hydro turbine designers.

Shear stress was one of the potential injury mechanisms contributing to fish mortality in the Kaplan turbines. Shear occurs when water interacts with the mechanical structure of the turbine and also when secondary flows are present in the mean flow.

Department of Energy in 1999 carried study to find the biological response of fish to the shear levels experienced in turbines. A quantitative description of the shear stress intensity appeared from test jet, which quantified the relation of the stresses to direct and indirect biological effects on fish.

Deschenes, C., and Fraser, R. [12] presented a review of current tendencies regarding measurements on models of hydraulic turbines and discussed how such tests can be used to improve the overall performance of hydraulic turbines, taking into account overall efficiency, lifetime expectancy and environmental issues. New strategies for funding major R&D projects of current concern were also discussed.

Present hydraulic market experience encounters strong pressures, both of a regulatory and a public driven nature, to mitigate environmental problems associated with hydraulic turbines, including reducing fish mortality by rendering existing or new units more “fish friendly” and compensating for dissolved oxygen depletion by turbine aeration. In addition, many powerhouses are ageing and in need of major overhauls.

This means that manufacturers have to develop machines that can be installed within existing civil constraints, whilst still providing proven efficiency or power

output, longer lifetime expectancy, and hopefully fulfilling new environmental requirements.

New trends in the energy market also include an increased concern to optimize the use and the benefits of existing hydro assets. To cover peak loads, turbines shall be operated more and more frequently in transient and unsteady modes. There is therefore a need to understand the effects of start / stop cycles on the life expectancy of the runners.

Major interdisciplinary research and development work has to be undertaken to achieve these objectives. Additional fundamental knowledge has to be garnered, at the frontier between biology, mechanics and fluid mechanics, on subjects as varied as fish and environmental responses, two phases flows, transient flows and fluid-structure interaction. A cooperative development of new experimental model tests and numerical simulations is required to get a better knowledge of the biological and physical phenomenon involved. The research literature shows for example that it is now possible to tackle some of these problems by measuring the velocity and turbulent fields inside model turbines using non intrusive methods such as PIV and LDV laser systems, and fast responding pressure measurements. Parallel prototype/model tests should allow us to develop better and more sophisticated scale-up formulae.

The tendency is now to form consortiums working on generic research and development projects, rather than specific ones, involving close partnerships between utilities, manufacturers, fluid researchers and environmentalists.

New emerging research and development preoccupations aim at developing better turbines and plants - more efficient, more robust and more environmentally friendly - for the benefit both of industry and people in the communities. It is believed that, by working in new ways and publicizing success stories, it will become possible to rejuvenate the image and perception of the hydro industry. This will attract the talented students and young engineers and researchers that are needed for industry worldwide.

Hydropower remained the most important renewable source for electrical power generation worldwide, providing 20% of the world’s electric supply [61].

Paish, O, et al. [2] summarised new innovations in the small hydro power technologies and the barriers to further development in the hydro turbines. Small hydropower is the most cost-effective technology to provide the hydr-electrification in the rural areas.

Small-scale hydro-power technology is extremely robust and is one of the most environmentally benign energy technologies available. It can last for more than 50 years with little maintenance.

Hydro power developments have been mostly associated with the dams in the 20th century. Because of energy issues globally, electric power demand is likely expected to increase more rapidly. After reviewing the tendencies of the energy market for the new generation, small and micro-power systems will be more effective and appropriate. The decision for building a hydro power plant must be based on the site potential, economical constraints, environmental issues and technological aspects.

Dragu, C., and Soens, J. [13] worked on the literature survey of the advantages and drawbacks of small and micro hydro power plants. Earlier special attention was given to the wind and solar power. Comparison with other renewable becomes very important.

High initial and low operating costs are the main economic characteristics of hydropower. From the studied literature, an easy algorithm can be proposed to assure the maximum efficiency for minimum costs of a hydro potential site.

Last decade has shown increase of demand for energy resources in all the economical sectors, where demand for electricity stands at the highest rate of growing. Position of the renewable technologies is expected to become more and more important in the global environment. .

Small-scale renewable generation being the cost-effective can bring electricity to remote areas which are far away from transmission lines.

To improve the design of a small hydraulic axial turbine, Jean-Louis Kueny, and Rémi Lestriez, [14] used an optimal design technique, based on artificial neural

network and genetic algorithm. The technique is first applied to the runner and cone geometry, taking in account the tip flow. The proposed objective function takes into account the runner losses and the kinetic losses at outlet and permits to fit the design to the projected flow rate. The final geometry used to optimize the runner corresponds to the runner, cone & draft tube. When the draft tube is taken into account, the best performance is obtained with a non negligible swirl at runner outlet, contrary to the no swirl solution at cone outlet obtained without draft tube.

Busea, C, et al. [15] carried research work on studying the axial hydraulic turbine runner optimization using the finite element analysis software. Using the CFD simulation, with less response time, modification can be investigated in a short time. Latest CFD techniques can predict energetic characteristics with certain accuracy level, as fluid simulation techniques do not replace experimental tests in precise.

Ferrando, L, et al. [16] worked on the application of a surface parameterization to a blade of Francis runner turbine. This geometric representation should be used as a practical tool in the process of design optimization. Most parameterizations are based on blade section approaches. The parameters are typically angles, lengths that have a clear meaning to the hydraulic designer. Span-wise functions are sometimes used to ensure coherence between the sections and the smoothness of the constructed blade surfaces.

In this case, the section-to-section approach was replaced by a purely surface method. The blade is modelled using a camber surface and thickness distributions, and the design parameters are kept as close as possible to their original physical meaning. Smooth blade surfaces are ensured, and a reduced number of variables is sufficient to describe realistic designs. Their line of research aimed to introduce a surface parameterization approach which provides a representation of the blade. One of the benefits of this methodology is the reduction of design parameters involved as this approach is no longer section dependent.

Other advantages reside in the easiness to obtain smooth geometries. Finally, it is also important to point out that data exchange between programs (i.e. CAD, Mesh Generator) may now use surface representation.

This entails that subjective reconstruction of this surface is no longer necessary. As a conclusion, with their approach and the reduction of design parameters, the design optimization process becomes shorter in terms of time and effort.

In order to handle all requirements for development of turbines, the technical-economic analysis is unavoidable. Computational Fluid Dynamic (CFD) simulation can be a complement to model testing and help us to speed up the design procedure. Tiaple, Y., and Nontakaew, Y. [17] carried design study of hydro turbine suitable for the specific site of Lower Mae Ping dam. The design concerned several constrains i.e., the existing civil structure of the dam, the flow regulation for irrigation and the limitation of water level that can effect to the efficiency of hydro power plant at upper dam. The optimizations for all purposes were considered. These design procedures can be applied to most of hydro power resources.

Hydro-power energy can play an important and critical role among sustainable renewable re-sources. Cross-flow type is suitable choice and viable solution from technical and economical point of view among different types of hydraulic turbines.

Barglazan, M et al. [18] worked on the design optimization of cross flow turbines by establishing optimum values for some geometric parameters of the cross-flow turbine. It was focused on the radial runner and the supply nozzle.

Automated design of the cross-flow hydraulic turbines was obtained through computer programs in which some parameters could be chosen as input data and some parameters can be calculated.

In hydropower generation the push towards lower cost and more flexible output leads to the demand for more compact machines and a larger required operating range for new and upgraded turbines. As a result hydrodynamic effects in turbines such as the draft tube rope at part load and the wicket gate runner blade interaction become important issues in the design of these machines.

Presence of the vibrations from the rotor-stator interaction in high head Francis runners is known phenomena. In the past, some of the vibrations resulting from this interaction have been attributed to a phase resonance phenomenon in the radial passages of the turbines [19-20]. According to these publications strong machine vibrations occur because pressure waves generated by the interaction between individual blades and wicket gates propagate circumferentially in the radial spaces. If these waves are in phase, they amplify and can cause problematic levels of vibration. In some cases where site observations report strong vibrations no correlation can be made with phase resonance [20]. In those cases he supposes the wicket gate-runner blade interaction to be directly responsible. More recently the hydrodynamic wicket gate-runner blade interaction has been found to be directly responsible for blade cracking [65].

Extensive work on rotor-stator interaction has been done in the field of acoustics. In thermal turbo machines determining which modes form and propagate, therefore contributing to the acoustic field is of primary concern [22]. For the structural response of hydraulic turbines to rotor-stator interaction the modes and mode shapes are as important as in machine acoustics, which has been studied extensively by Tanaka, H., et al. [23]

Coutu, A., and Velagandula, O., [21] have reported on a method to predict the forced response of a hydraulic turbine due to rotor-stator interaction. Arndt et al, [24] carried investigation on the interaction between diffuser and the impeller of a hydraulic pump. Authors performed the unsteady pressure measurements to discover the large pressure amplitudes, which decreased significantly with an increasing radial gap.

Dring et al. [25] performed experimental study on the rotor-stator interaction in a gas turbine stage and discovered large pressure amplitudes in both the rotor and the stator channels. Steady state Computational Fluid Dynamics (CFD) analyses have been an integral and well validated part of the hydraulic design procedure at GE Energy Hydro for many years [63]. However, only recent developments in CFD software [27] and affordable computer technology – notably the availability of Linux clusters for parallel computing – have made the

simulation of the unsteady flow field possible, opening the door for the prediction and understanding of unsteady flow phenomena [26].

Williams, A.A., and Simpson, R.G., [28] worked on research project for developing standard design procedure for pico propeller turbines for local manufacturing in the developing countries. A 5 kW demonstration turbine was set up at a test site in Peru. Computational Fluid Dynamics (CFD) has been used to obtain overall performance data for the turbine and to assist in the design of a new rotor.

It was found that an incorrect matching between the rotor design and the available flow rate at the site significantly affected the turbine operation and in order to provide an acceptable performance it was possible to adjust the runner design and operating speed of the turbine. Authors concluded that the computational fluid modelling can be used as an appropriate design tool.

Jingchun Wu, et al. [29] applied it to a Francis turbine rehabilitation project to provide over 3% increase in peak efficiency and improved cavitations characteristics. Simulations were performed for both the existing and for the new turbines at design and off design conditions. For interactions between rotating and stationary parts, coupling calculations based on the implicit coupling method were carried out for the entire turbine model to optimize the runner and guide vanes. Stay vanes were locally developed with minimum cost under the geometrical constraints of the existing machine. The performance of the new design was verified through the model tests.

In very old Francis hydro turbine units, frequent repairs of the cavitations damage destroyed regular flow passage, leading to drastic deterioration of turbine performance. As a result, these turbines do not generate their rated capacity. It is, therefore, strongly desired to rehabilitate the turbines with new runners using modern design methods to update the efficiency, raise the capacity and improve the cavitations characteristics. Runner replacement projects of this kind present a great challenge for hydraulic design because of the geometrical constraints of the existing machines. Recently, with the rapid development of computer technology and advanced CFD, it has become routine to directly simulate internal turbulent flow in individual or multiple components of a turbo-machine.

Cruz, et al. [30] carried research on the application of minimum pressure coefficient criteria for the axial-flow hydraulic turbines cascade geometry design. In recent works, the criteria was tested for the axial fan, showing that it is suitable to define the initial geometry for machine design. The global parameters that supply the principal dimensions of the turbine were obtained from the literature as based upon statistical data of installed power plants.

The simulation domain grid was generated with CFX-TURBO. Results were obtained to analyze the fluid flow through blade runner. In this way, a study was carried out on a small axial-flow turbine specifically designed for operating in small rivers.

Keck, H., and Michler, W., [31] studied different methods for life cycle analysis based on the dynamic loading. Validated pressure pulsations resulting from CFD have shown prediction of pressure load as input to the structural analysis of the runner.

Risberg, S., and Jonassen, M. [32] carried out the demonstration work on the use of a surrogate model based approach for Francis turbine runners design. Authors took the benefit from a new parametric definition of the Francis turbine runner blade in combination with CFD and FEM simulations. This model is useful way for attaining insight into the global behaviour of various runner profiles.

Common blade Francis runners were under development based on this approach with new design. It ensures a systematic and continuous philosophy to optimize the runner profiles according to the actual flow and head given by the nature in each specific project.

V.C. Campian, et al. [33] carried the study on failure analysis of a Kaplan turbine runner blade from a hydropower plant. Authors carried out metallographic investigations on the sample taken from the cracked piece of blade. The metallographic investigations included microscopic examinations as well as X-ray diffraction analysis. It was found that the cracking of the blade started and developed from the stress concentration between blade and blade flange on leading edge direction.

To decrease the maximum stress values, authors suggested reducing the hydrodynamic loads on the blade. The stress reduction could only be done by increasing the number of the runner blades, as the operating conditions like discharge, head, speed, and power were not changeable.

It is not possible to carry out the experiment on prototype hydro-turbine, before the power plant is ready. Rational prediction of the pressure fluctuations is very important in the prototype turbine during design phase.

ShuHong, L., and Jie, S., [34] treated the unsteady turbulent flow computation based on the modified turbulence model through the flow passage to simulate the pressure fluctuations.

The conventional method to assess turbine performance is its model testing which becomes costly and time consuming for several design alternatives in design optimization. Computational fluid dynamics (CFD) has become a cost effective tool for predicting detailed flow information in turbine space to enable the selection of best design.

Prasad, V., and Gahlot, V.K., [35] carried out the 3D real flow analysis in an experimentally tested axial flow turbine and different flow parameters were computed at three operating regimes to find the best operating regime. The computed efficiencies were critically compared with experimental values and found to bear close comparison.

In axial flow turbine, water passes through the series of blade rows and changes its direction from radial to axial. Runner is the most important component of the turbine and its blade profile is designed at different sections from hub to casing to get the best performance. The rotation of runner and operation of turbine either below or above the rated conditions cause variation of flow parameters from hub to tip [36], [60].

Hence, actual flow pattern in turbine space deviates from the simplifying assumptions made in design thus affecting the turbine performance. The experimental testing of turbine models at different operating regimes on specially designed test rigs is the conventional approach to assess the performance. But this approach provides global performance at varying

operating conditions and does not give detailed information about the flow behaviour and variation of local design parameters like blade circulation, lift and degree of reaction. The model fabrication and testing for any change made in design make this method costly and time consuming.

The combination of advanced numerical techniques and computational power has lead to computational fluid dynamics (CFD). It is an efficient and inexpensive tool to make internal flow predictions to good accuracy and, any sort of flow problems can be detected and further improvements can be made on the geometry of turbine components. It has made possible to obtain a significant enhancement in efficiency [37-40].

CFD can be used to check efficacy of alternate designs [41-42] of turbines for optimization before final experimental testing of selected designs is resorted. However, in order to prove reliability of these tools for application to turbines, validation [43-45] with known experimental results is required. The variations of flow parameters from hub to tip of runner are presented in graphical form and average value of cascade parameters are computed at different operating regimes. The computed efficiencies have been compared with experimental values at three regimes for validation of simulation results.

Singh, P., et al. [46] carried study for the development of hydraulically optimized solutions of the propeller turbines for micro hydro range focusing on the simple manufacturing. Author presented range of geometrical optimization steps carried out on a propeller runner. Blades were designed using the free vortex theory having gross head from 1.5 to 2 m with water flow rate of around 75 litres per second. Three stages of geometrical modifications carried out on the runner aiming to optimize the runner performance. This study presented an interesting theoretical methodology for analyzing the effects of each optimization stage.

Performance of the runner was found very sensitive to changes to exit tip angle. At two modification levels, the discharge increased from 15% to 30%, while shaft power increased from 12% to 45%, influencing the efficiency characteristics. Runner inlet tip modification results were very interesting. In this case, significant rise of turbine efficiency was recorded at the best

efficiency point, which was caused by reducing the discharge consumption as well as higher power generation.

Optimization study on propeller runner has validated the estimates of the free vortex theory despite small deviations. Final runner configuration demonstrated maximum efficiency of around 74%, which is very encouraging from the perspectives of micro hydro application. It concluded with recommendations of a series of optimization steps to increase the efficiency of the runner. It also recommends the attempt of Computational Fluid Dynamics both as a validation and optimization tool for future research on propeller runners.

Khare, R., et al. [47] carried simulation of three dimensional flow in a mixed flow (Francis) turbinee using ANSYS CFX 10 to study the flow pattern in the turbine. Futher work was done on the computation of various losses and efficiency at different operating conditions.

Helena, M.R., and Mariana. S., [48] conducted research on hydro turbines for optimization and the selection of adequate hydro turbines. The hydrodynamic fluid mechanical analysis require the use of complex advanced models which apply the equations of Navier-Stokes by using mathematical models of conservation laws, for the study of the turbulent flow behaviour. To determine the correlation between the flow velocity and pressure fields, they used k-ε model.

They aimed to search for new solutions regarding the energy production of available low power in water systems. The hydropower equipment known as micro-hydro, represents an advantageous economic alternative in terms of hydroelectric exploitation in water systems, when compared with dissipative structures.

This type of energy associated to low power production and the financial search have been very conservative in what concerns the development of micro turbines, in alternative to major powers. With the purpose of providing and developing future areas with energy potential, especially in developing countries, rural or isolated areas, the use of micro-turbines can promote the economical development and the creativity for designing new solutions.

With the objective of promoting the use of energy associated with the installation of low power systems (i.e., low heads and/or discharges), for example in water systems supply or irrigation, the hydrodynamic flow through the selected turbines to these conditions and the estimation of the best efficiency point, with the aim of finding new possible applications in systems already existent, can be developed.

Nicolle, J., and Labbe, P., [49] used computational fluid dynamics for analysis purpose on the performance of existing turbines. Two different geometries were used for demonstration, one propeller and the other Francis turbine.

Paik, N.C., and Byeon, S.S., [50] carried research work to optimize the axial propeller turbine operating with 3~6 m water head. Three stages of optimization were executed for the turbine with the geometrical modifications by varying the number of runner blade, pitch angle and three different blade profiles. In their study, they attempted to acquire basic design data, the output power, efficiency and pressure distribution to suggest the sound method of optimization.

Sutikno, P., and Adam, I.K., [51] carried out research in order to develop a hydro turbine to be used for specific site of lower head of less than 1.2m. Development of very low head turbine has been done in this research using the simple civil construction and economically viable. The recent development of computational techniques has allowed a substantial improvement in hydraulic turbine design. Initial geometry capable to assist certain characteristics of turbine performance is step for useful numerical turbine analysis.

GAMBIT grid software package was used to generate the grid of the simulation domain and results were obtained using the 3-D FLUENT flow to analyze the fluid flow through blade runner. Study was carried out on a small axial-flow turbine, specifically designed to operate in a very low head and finally evaluating the results for hydraulic efficiency prediction of the turbines. The prototype of turbine system was tested by using small channel system. Tested result was obtained for maximum efficiency of 90% and the power output simulation and experimental has the differential less than 5%. Hydraulic turbine design involves many stages of iterative calculations.

Thapa, B.S., and Panthee, A., [52] carried out study to simulate the design and operational problems of Francis and Pelton turbines by the application of computational tools. A new program was developed to optimize designs of Francis runners for sediment erosion problems and CFD analysis of some new design conditions was done. True size Pelton runner model was developed by using Solid Works for stress and fatigue analysis by using Cosmos Works in its operating conditions.

It was found that numerical models are capable to simulate the design and operational problems in hydro turbines. The computational tools can also suggest the design optimization needed to minimize these problems. It was observed that sediment erosion in Francis turbines can be reduced up to 50% by optimizing the hydraulic design.

After detailed literature review and survey on the hydro-power development, it was concluded to focus to carry research work on the development of low head hydro turbine runner blades to acquire maximum power output through the geometrical changes in the profile structure using CFD.

CHAPTER 3

3 DESIGN AND DEVELOPMENT OF RUNNER

3.1 Introduction

Hydro turbines contribute the most important part for hydro-power generation in the world. Different types of turbines can be used for range of heads and water discharge. Kaplan turbines are mainly used for low head applications.

For any specific hydro site, head of water and unit rate of water flowing provide the information of the expected power available with suitable selection of turbine type.

Most recommended and suggested material for the manufacturing of hydro turbine blades is ASTM A743 CA6NM martensitic stainless steel [53-54]. This material is suggested based on its better strength, resistance ability to cavitations, easily to cast and fabricate, weld-able and capable of erosion protection. Its mechanical properties are adequate for use in water turbines [55].

3.2 Basic Design Model

Based on the site data, basic design of the Kaplan turbine is illustrated.

Maximum level of water = 766.60 ft SPD

Minimum level of water = 744.60 ft SPD

Net head of water, H = 6.7 m

Discharge of water, Q = 3100 ft^3/sec (87.73 m^3/sec)

ρ = 998 kg/m^3

g = 9.81 m/sec^2

Hydraulic efficiency, η_h = 0.80

Power output, $P = Q.H.\rho.g.\eta_h = 4{,}603{,}758$ Watt

P = 4.60 MW

3.3 Development of CAD Model

Basic data of Kaplan Turbine is obtained from the Nandi-Pur Hydro Power Plant i.e. design flow rate of 87.73 m^3/sec (or 3100 ft^3/sec), net head of water of 6.7 meters with approximately 80% efficiency.

Main characteristics of the turbine are ;

Maximum power output = 4.6 MW

Runner diameter = 4.24 m, and

Hub diameter = 1.76 m

Typical plan view of the runner-blade assembly is shown in Figure 3.1

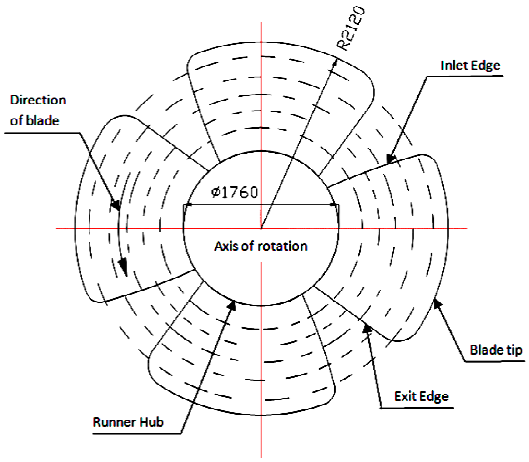

Figure 3.1: Plan view of runner blade assembly

Development of the complex shaped three dimensional models of turbine blades is very essential to proceed further for optimization of the blade profiles by utilizing the computational fluid dynamics analysis.

For this purpose, blade profile of original sample is used to create the CAD solid model from the as-built geometry. Profile geometrical data was developed in the form of coordinate points in x-axis, y-axis and z-axis. It was

taken on the true levelled test bench at the shop floor. Development of the complex blade geometry for initial design have been carried out in AutoCAD and Pro-E / Creo based on the data acquired.

3.3.1 Development of CAD Model – CASE A

Coordinate-measuring machine (CMM) and 3D scanner are now-a-days commonly used for measuring the physical geometrical characteristics of an object for the development of complex CAD models in the industry as well as in the academic institutes. Pro-E / Creo have been utilized to develop CAD models of turbine runner blade with the help of coordinate points system. Through this procedure, different CAD models of blade profiles with required geometries were possible to be developed.

Points were measured physically from the runner blade on test bench i-e surface table by using the well calibrated measuring instruments like height gauges to ensure the accuracy of the measurements taken by qualified quality personnel. True levelled surface of the test bench was taken as reference for these measurements.

In this procedure, runner blade was placed and levelled on the test bench / surface table. Blade upper and lower surfaces were properly cleaned before marking of points. Outer periphery of the blade on upper and lower sides was measured by using calibrated measuring tape. At start, initial reference point was marked as coordinate (0, 0, 0) and from this reference point, next point was marked on the periphery line at an interval of 100mm with the help of divider. This point was then measured with respect to initial point by measuring the dimensions along x-axis, y-axis and z-axis.

Dimensions along x and y axis were measured with the help of calibrated Vernier Calipers, whereas dimension along z-axis was measured by using the calibrated height gauge. In this way, all the points / coordinates were measured and plotted on the drawing.

Table 3.1 shows the coordinates for hub side of the blade geometry, Table 3.2 shows the coordinates for shroud side of the blade geometry, Table 3.3 shows

the coordinates for leading side of the blade geometry and Table 3.4 shows the coordinates for trailing side of the blade geometry.

Table 3.1: Coordinate points for hub side (case – A)

	Hub side - upper edge		
Point	X-axis (mm)	Y-axis (mm)	Z-axis (mm)
1	650	-1527	18
2	600	-1476	38
3	500	-1396	76
4	400	-1336	115
5	300	-1293	155
6	200	-1263	205
7	100	-1246	251
8	0	-1240	291
9	-100	-1246	326
10	-200	-1263	356
11	-300	-1293	378
12	-400	-1336	405
13	-464	-1372	422

	Hub side - lower edge		
Point	X-axis (mm)	Y-axis (mm)	Z-axis (mm)
1	650	-1527	5
2	600	-1476	10
3	500	-1396	22
4	400	-1336	33
5	300	-1293	44
6	200	-1263	58
7	100	-1246	81
8	0	-1240	114
9	-100	-1246	158
10	-200	-1263	213
11	-300	-1293	280
12	-400	-1336	347
13	-464	-1372	391

With the help of coordinate points measured physically, blade geometries were plotted to develop the proper drawings. drawings And with utilization of the coordinate system. Sequence of working on the drawings to develop final CAD 3D model is as shown in Figure 3.2, Figure 3.3, Figure 3.4 and Figure 3.5.

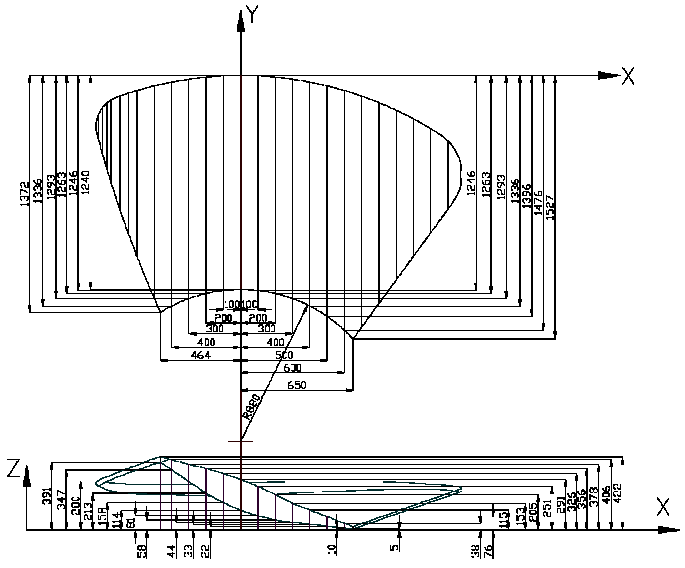

Figure 3.2: Development of drawing for hub side upper/lower edge

Figure 3.2 shows the developed profile of blade on hub side. Dimensions indicated in the drawing are tabulated in Table 3.1. This data is then used as points input for Pro-E/Creo to generate the outlines on hub side.

Table 3.2: Coordinate points for shroud side (case – A)

	Shroud side - upper edge				Shroud side - lower edge		
Point	X-axis (mm)	Y-axis (mm)	Z-axis (mm)	Point	X-axis (mm)	Y-axis (mm)	Z-axis (mm)
1	-100	-2	268	1	-100	-2	197
2	-200	-10	266	2	-200	-10	199
3	-300	-21	263	3	-300	-21	200
4	-400	-38	263	4	-400	-38	204
5	-500	-60	262	5	-500	-60	207
6	-600	-87	264	6	-600	-87	209
7	-700	-119	269	7	-700	-119	218
8	-750	-140	272	8	-750	-140	227
9	-775	-158	274	9	-775	-158	232
10	-800	-185	278	10	-800	-185	243
11	-825	-229	283	11	-825	-229	255
12	0	0	273	12	0	0	205
13	100	-2	265	13	100	-2	204
14	200	-10	264	14	200	-10	207
15	300	-21	264	15	300	-21	214
16	400	-38	263	16	400	-38	218
17	500	-60	262	17	500	-60	222
18	600	-87	261	18	600	-87	226
19	700	-119	260	19	700	-119	229
20	800	-157	259	20	800	-157	232
21	900	-201	258	21	900	-201	235
22	1000	-251	258	22	1000	-251	236
23	1100	-308	257	23	1100	-308	235
24	1200	-379	256	24	1200	-379	230
25	1250	-447	256	25	1250	-447	231
26	1270	-497	247	26	1270	-497	231
27	1281	-569	240	27	1281	-569	230

Figure 3.3 shows the developed profile of blade on shroud side. Dimensions indicated in the drawing are tabulated in Table 3.2. This data is then used as points input for Pro-E/Creo to generate the outlines on shroud side.

Developed profile of blade on leading edge is shown in Figure 3.4. Dimensions indicated in the drawing are tabulated in Table 3.3. This data is then used as points input for Pro-E/Creo to generate the outlines on leading edge.

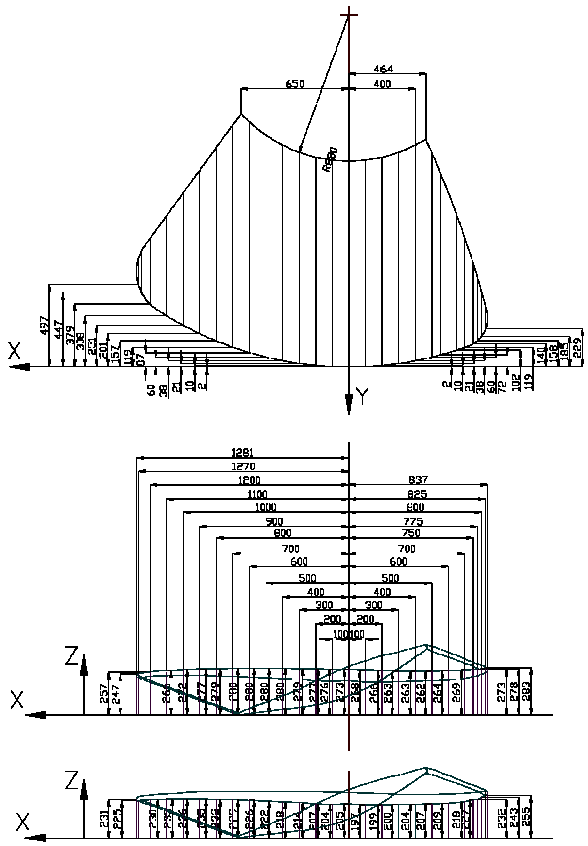

Figure 3.3: Development of drawing for shroud side upper/lower edge

Table 3.3: Coordinate points for Leading side (case - A)

	Leading side - upper edge				Leading side - lower edge		
Point	X-axis (mm)	Y-axis (mm)	Z-axis (mm)	Point	X-axis (mm)	Y-axis (mm)	Z-axis (mm)
1	-837	-295	275	1	-837	-295	243
2	-825	-365	283	2	-825	-365	251
3	-800	-455	293	3	-800	-455	261
4	-775	-541	303	4	-775	-541	271
5	-750	-623	314	5	-750	-623	281
6	-700	-776	333	6	-700	-776	301
7	-650	-918	353	7	-650	-918	321
8	-600	-1050	372	8	-600	-1050	340
9	-550	-1174	391	9	-550	-1174	358
10	-500	-1292	409	10	-500	-1292	377

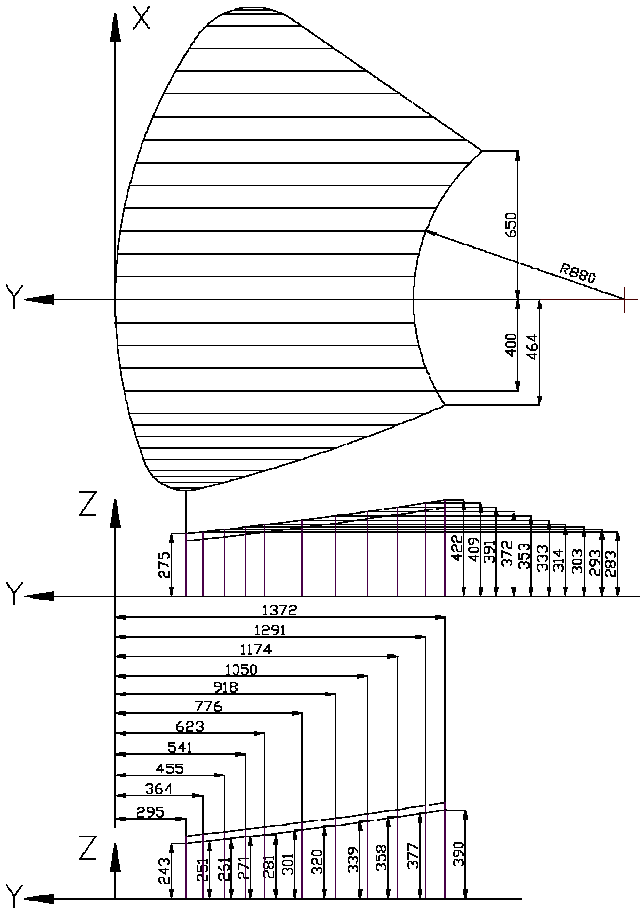

Figure 3.4: Development of drawing for leading side upper/lower edge

Table 3.4: Coordinate points for trailing side (case - A)

	Trailing side - upper edge		
Point	X-axis (mm)	Y-axis (mm)	Z-axis (mm)
1	1270	-650	221
2	1250	-700	210
3	1200	-774	192
4	1100	-911	161
5	1000	-1048	129
6	900	-1185	97
7	800	-1322	66
8	700	-1459	34

	Trailing side - lower edge		
Point	X-axis (mm)	Y-axis (mm)	Z-axis (mm)
1	1270	-650	208
2	1250	-700	196
3	1200	-774	179
4	1100	-911	147
5	1000	-1048	116
6	900	-1185	84
7	800	-1322	52
8	700	-1459	21

Figure 3.5 shows the developed profile of blade on trailing edge. Dimensions indicated in the drawing are tabulated in Table 3.4. This data is then used as points input in Pro-E/Creo to generate the outlines on trailing edge.

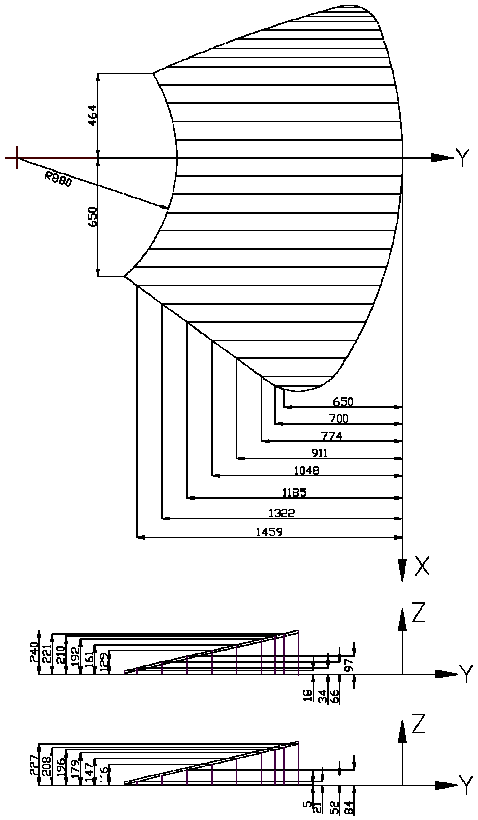

Figure 3.5: Development of drawing for trailing side upper/lower edge

3D model of the blade profile have been developed with the help of coordinate points. Further to carry out the CFD study on the similar blade profile, four different profile structures were re-designed and developed based on different inclinations / angles. These four profile structures were named as Case-B, Case-C, Case-D and Case-E.

Coordinate points for the development on hub, shroud, leading and trailing edges of blade profiles for case-B, case-C, case-D and case-E are illustrated in Appendix-A.

For case-B, coordinate points for hub and shroud are tabulated in Table A-1 and for leading and trailing side in Table A-2. For case-C, coordinate points for

hub and shroud are tabulated in Table A-3 and for leading and trailing side in Table A-4.

Similarly for case-D, coordinate points for hub and shroud are tabulated in Table A-5 and for leading and trailing side in Table A-6. For case-E, coordinate points for hub and shroud are tabulated in Table A-7 and for leading and trailing side in Table A-8.

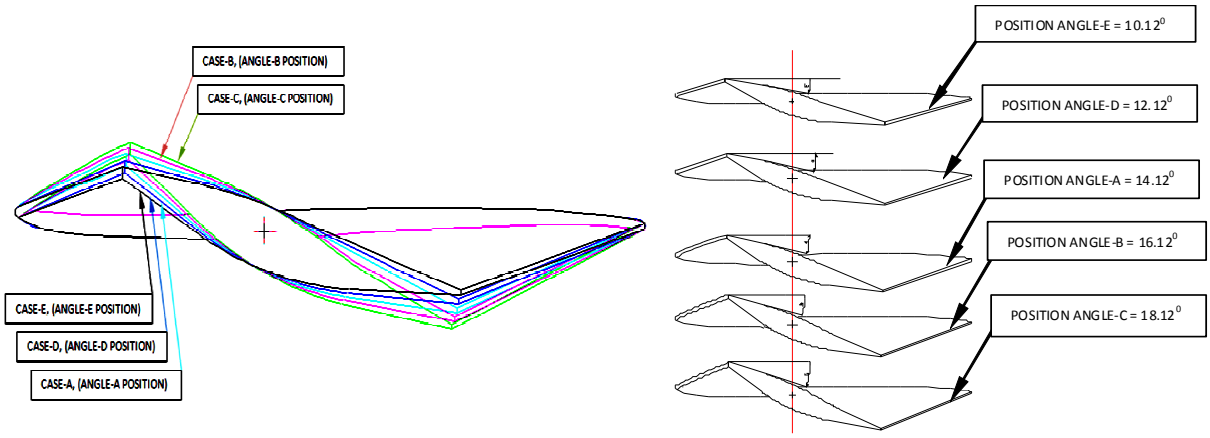

Figure 3.6: Development of blade geometry at different angles

Further these blade profiles were analysed using CFD in ANSYS – CFX module from optimization point of view. Many researchers / investigators have already used the computational fluid dynamic techniques for analysis and validation of the hydro turbine components [29], [35], [56].

4 MANUFACTURING OF BLADE

In this chapter, complete procedure for the production of Kaplan turbine runner blade is described. Blade have material properties of low carbon high chromium nickel as per material grade of ASTM A743 grade CA6NM.

4.1 Production Route of Runner Blade

In this section, production methodology of the runner blade has been discussed in detail.

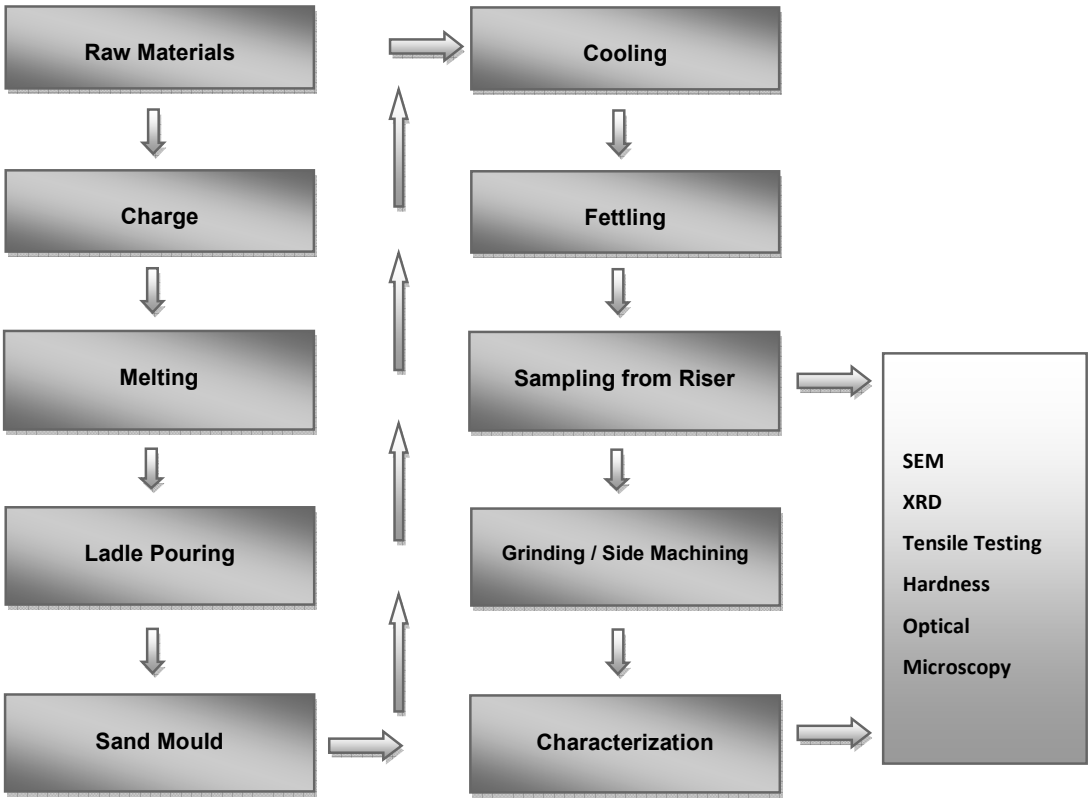

Figure 4.1: Work plan for blade manufacturing process

4.2 Raw Materials

The manufacturing of high alloy steel requires large amounts of expensive alloying elements, which are the main factor influencing the total production

cost. As regards utilization of alloy scrap, conventional steelmaking practices in electric arc furnaces had not ensured required very low content of carbon in stainless steel, in view of carbon pick-up due to the use of graphite electrodes.

Decarburization of high chromium-steel is very complicated. Intensive oxidation of chromium occurs in lower temperatures of metal bath, while for carbon oxidation much higher temperature is necessary. Therefore, decarburization of steel without significant losses of chromium is not possible. Also, the rate of chemical reactions is low and leads towards increased refining time and thus higher consumption of furnace refractory.

The above mentioned problems can be avoided when special processes like Argon Oxygen Decarburization (AOD) and Vacuum Oxygen Decarburization (VOD) are used for stainless steel production.

4.2.1 Procedure:

To produce low carbon stainless steel with modified manner of intensive oxygen blowing into a metal bath. This method allows achieving low carbon content and prevents high losses of chromium at the same time. It is possible to utilize all kinds of high Cr and Cr-Ni scrap with satisfactory economical results.

The intensive oxygen lancing gives the opportunity to carry out the refining of steel in temperatures approximately 200°C higher, as compared to conventional practices. In short time, the temperature, reaches above 1800°C changing the course of oxidation reactions. In such conditions, the dissociation pressure of carbon mono-oxide increases slower than pressures of Cr, Mn, Fe and Si oxides dissolved in slag.

4.3 Raw Material Processing:

1. Furnace charge was composed of 70-80% of alloy scrap and 20-30% of carbon steel scrap (or low alloy steel scrap). Chromium content at melt-down rather was aimed not to exceed 14%, otherwise losses of Cr may be higher than it is expected.
2. Since a rapid increase of temperature does not facilitate dephosphorization, therefore phosphorus content in the charge was

kept below required limits for the specified steel grade. Clean (so called "blue") scrap was used in the production of blade.

3. Melt-down carbon and silicon was kept around 0.3% and 1.0% respectively. As regards silicon, it is assumed that the charge should include a compound which is a "fuel" enabling fast increase of the temperature at the beginning of the process.
4. Oxygen lancing starts when the metal bath temperature is above 1600°C. Required oxygen pressure is 6-10 atmospheres, total lancing time 15-30 minutes. Average oxygen consumption is 20-40 cubic meters per one ton of liquid steel and depends on carbon content before and after oxidation.
5. As a reducing materials for chromium recovery from slag after oxidation, ferrosilicon, ferrosilicon-manganese, silicochromium and grinded aluminium were used.
6. During the reducing period, high temperature of metal bath was kept lowered up to the possible limits. It was achieved in the following ways:
    a. addition of the main portion of low carbon ferrochromium,
    b. addition of clean scrap of the same steel grade,
    c. tapping of steel and its return back to a furnace for further refining.
7. Desulphurization was carried out under the white slag (lime added).
8. Due to very high content of alloying elements, it may happen that a sample taken for chemical composition analysis in fact differs from the real (and expected) composition of steel. The ideal homogeneity of steel chemical composition can be achieved only in case of implementation of induction stirring or inert gas (Ar, N_2) blowing, which was done in the described manner.
9. Walls of a furnace used for stainless steel melting were made of high quality magnesite refractory. High alumina bricks were used in the roof.

4.4 Melting

Melting and casting of the charge materials with weighed quantity was done by electric arc furnace using graphite electrodes. Argon gas used to clean the chamber for removal of oxygen. After melting, it was analyzed in the melt down sample.

The steel was processed when the required composition was achieved as above. The pouring was done at the temperature 1600 ^{0}C for final casting. The casting was allowed to cool in the sand mould up to optimum temperature. After this the runner blade was shifted to the steel cleaning for fettling.

Total charge of 2600 kg consisted 2000 kg of 18-8 steel scrap, 450 kg of non-alloy scrap, 150 kg of ferronickel (60%). 15 kg of coke or broken electrodes and 80 kg of limestone were added before scrap charging. Assumed final weight of the melt was 3200 kg.

4.4.1 Operations:

1. 30 minutes before melt-down: addition of 40 kg 75% FeSi (in lumps)
2. Melt-down sample: 0.35%C, 1.2%Si, 0.78%Mn, 0.035%P, 0.030%S, 2.0%Ni, 2.0%Cr, 0.20%Mo
3. Removal of slag (80-90%)
4. Addition of 30 kg of fluorspar
5. Temperature check-out: >1600°C
6. Oxygen lancing: start and check time for (5-10 minutes) up to carbon burning process (flames) and then wait for 15-25 minutes for the end of oxidation (white fumes over furnaces).
7. Sample: 0.06%C
8. Slag reduction:
   - addition of 6 kg of Al, 25kg of MnSi and 20 kg of FeSi (in lumps)
   - final slag reduction (until it becomes very thin) by means of FeSi powder (or Al powder) added in batches 3-4 kg in 5 minutes intervals.
9. Two samples (in 2 minutes intervals) and removal of the whole slag
10. Addition of 300 kg of Low Carbon (Carbon < 0.1%) FeCr ("in advance" – without sample results) for decreasing of the steel temperature
11. Sample results:
    - 0.04% C, 1.02% Mn, 0.17% Si, 0.035% P, 0. 025%S, 10.35% Cr, 10.25% Ni
    - 0.04% C, 0.98% Mn, 0.20% Si, 10.55% Cr, 10.31% Ni.
12. Calculations and correction of steel composition:

    Cr = 10.45 in 2600 kg - this corresponds to 8.49% Cr in 3200 kg.

Ni = 10.28 - this corresponds to 8.35% Ni

Desired contents in steel : 12.0% Cr and 4.0% Ni.

Necessary additions:

- 10.31 % Cr (i.e. 485 kg of FeCr) including 300 kg advance.
- 1.65% Ni (i.e. 90 kg of FeNi)

Total 575 kg (FeCr – 73%Cr, FeNi – 60%Ni)

Checking of the assumed final weight of steel:

- Initial charge (2600 kg) + ferroalloys (575 kg) = 3175 kg is ok.

For correction of steel composition 185 kg FeCr should be added.

13. In the meantime, deoxidation of slag is being carried out, by means of FeSi powder added in batches 2-3 kg for each 5-8 minutes. Colour of the slag should change from green to light-brown (usually, it takes about 30 minutes).
14. Stirring of the metal bath (no remains of un-dissolved FeCr)
15. Temperature check-out : 1650 °C
16. The last sample and adjustment of chemical composition (Silicon: for steels without titanium)
17. 5-10 minutes before tapping (ladle ready under tapping spout) removal of the whole slag.
18. Addition of 105 kg of 32% FeTi (calculated for 1.0-1.05%Ti in steel - the yield is 40-80%and depends on steel temperature and slag fluidity) in common with 40 kg of fluorspar
19. Stirring of the metal bath and Tapping

4.4.2 Chemical Composition of Blade:

Table 4.1 indicates both specified and achieved chemical composition of the blade material. Material of the blade conforms to stainless steel grade CA6NM with respect to chemical composition. Composition was achieved using optical emission spectrometer, spectromax$_x$.

Figure 4.2: Optical Emission Spectrometer - Spectromax$_x$

Table 4.1: Chemical composition of ASTM A743 Grade CA6NM

Element %	C	Mn	Si	P	S	Ni	Cr	Mo	Cu	Al
Specified	0.06 Max	≤ 1.00	≤ 1.00	≤ 0.03	≤ 0.03	3.5~4.5	11.5~14.0	0.40~1.0	-	-
Achieved	0.065	0.63	1.02	0.017	0.012	4.45	12.00	0.47	0.18	0.091

4.5 Sample Preparation

Two samples 300mm long from riser (as shown in Figure 4.3) were cut using gouging with flush of water.

Figure 4.3: Two samples from riser

From one sample, different specimens (as cast) were prepared to perform various tests i.e. Metallographic Testing, Tensile Testing and Hardness Test etc.

4.5.1 Microscopy:

Microscopic examination can be used to identify the defects of the casting, strength, cleanliness, and control of the material. Optical microscopy of the runner blade material was carried out to observe the microstructure of the product both in as cast and heat treated condition, which are summarised in the following section.

4.5.1.1 Optical Microscopy of Blade (As Cast):

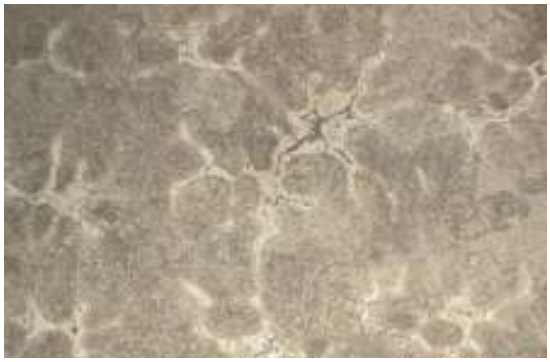

Figure 4.4: As-cast microstructure consist of carbide and ferrite present at prior Austenite grain boundaries in a matrix of martensite – X350

4.5.1.2 Scanning Electron Microscopy of Blade (As Cast):

Images of the scanning electron microscopy of the test piece are shown below.

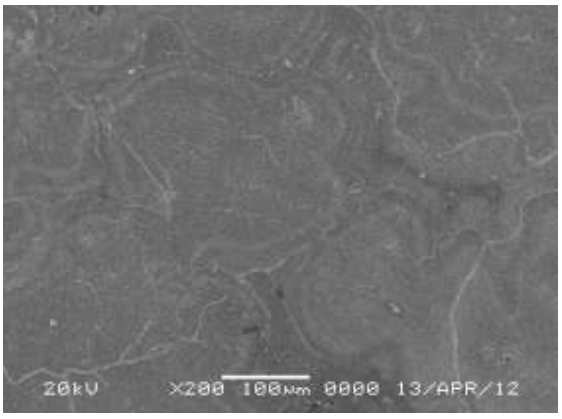

Figure 4.5: Micrograph of electron microscope at low resolution (x200), Carbides are not well resolved.

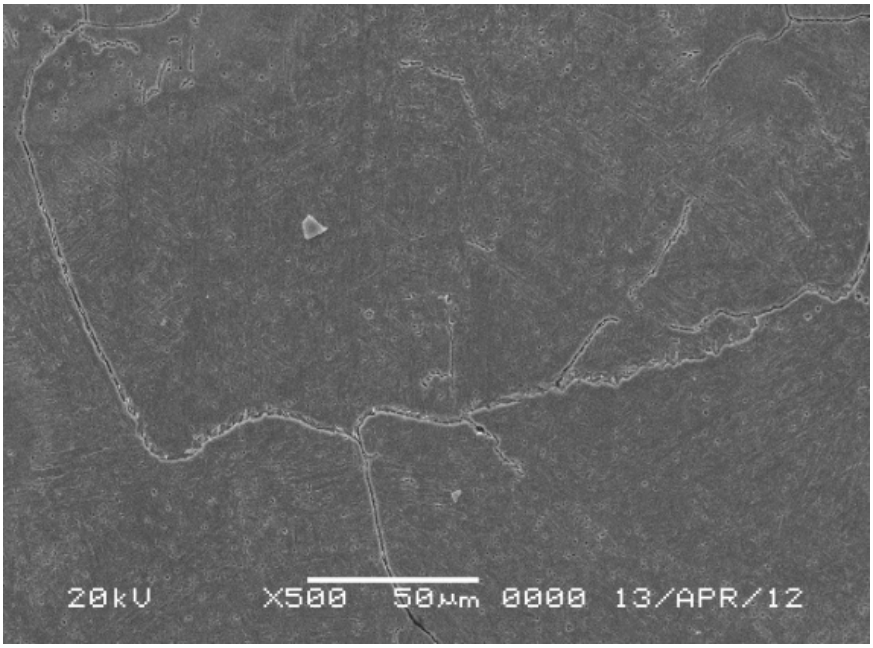

Figure 4.6: Micrograph of electron microscope at higher magnification (x500), carbides are better resolved.

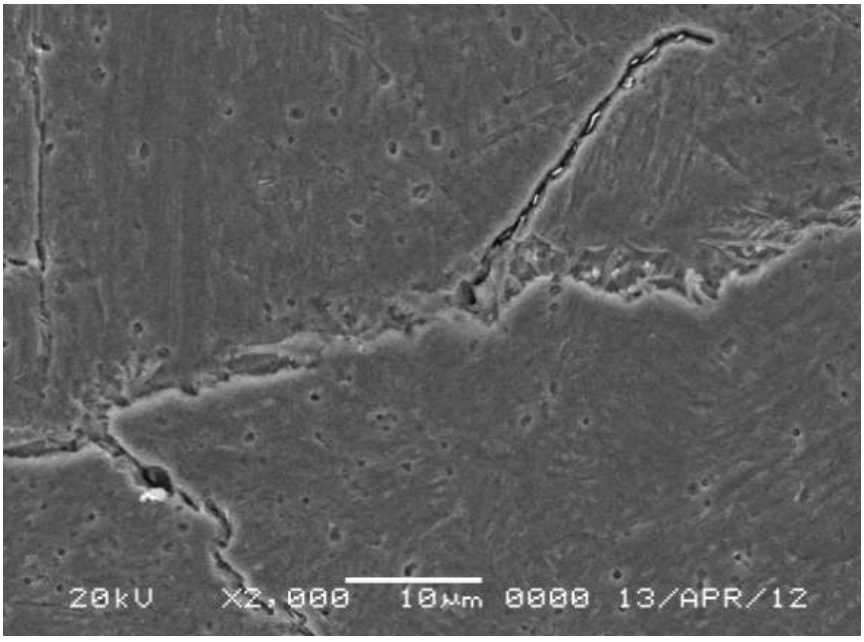

Figure 4.7: Micrograph of electron microscope of more higher resolutions (x2000), carbides are very well resolved as well as ferrites.

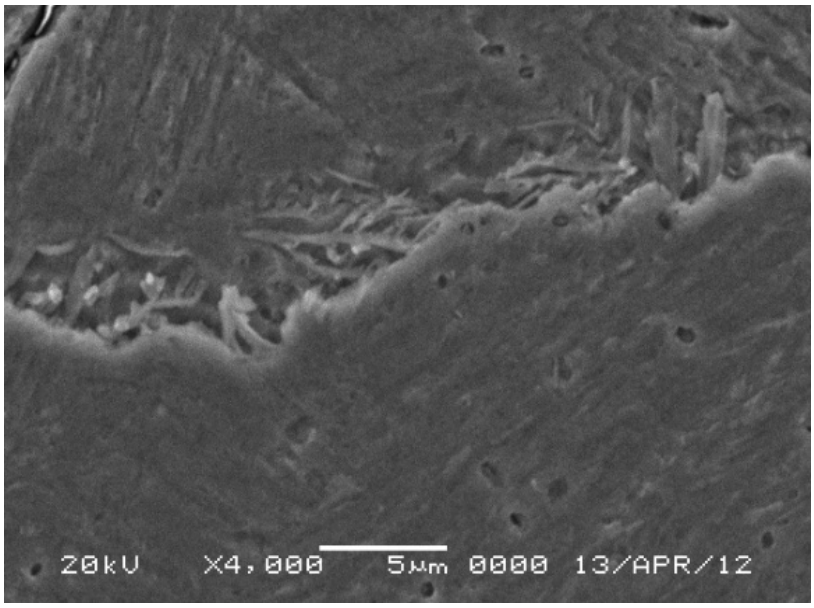

Figure 4.8: Micrograph of electron microscope with magnification x4000 indicating carbides, ferrites at grain boundary still more clearly resolved.

4.6 Heat Treatment

Other sample was heat treated for solution annealing as per heat treatment curve as shown in Figure 4.9. Furnace with suitable monitoring and controlling system was used. From this heat treated sample, various specimens for the test i.e microscopy, hardness, tensile testing was prepared and the results achieved are numerated in relevant sections.

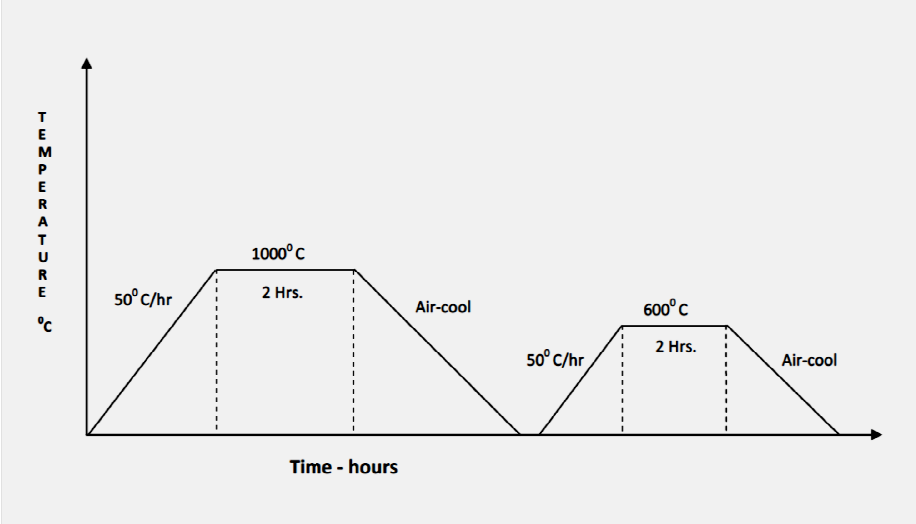

Figure 4.9: Heat Treatment Curve.

4.7 Test / Results of Heat Treated Material/Sample

Metallographic examination of the heat treated sample was carried on two different types of microscopes i.e. Optical Microscope and SEM (scanning electron microscopy)

4.7.1 Optical Microscopy of Blade (Heat Treated)

- **As polished**

  The specimen was then grinded up to 1000 grit size and then polished. To observe the non-metallic inclusion contents as per ASTM E-45. Results are shown in the figure 4.10

Figure 4.10: Oxide type Inclusions: as-polished specimen X100

- **Etched**:

  The specimen was etched in equal parts of concentrated HCl and HNO_3. Micro-structure was observed optically by using Meiji-7530 microscope.

Figure 4.11: Microstructure: tempered martensite X350

4.8 Mechanical Properties

4.8.1 Hardness:

Hardness of as cast and heat treated samples was checked using HBRV-187.5 Rockwell hardness tester at 150 kg loading. Results are shown in Table 4.2 below.

Table 4.2: Results of Hardness Test

Condition	Hardness
As Cast	44 HRC
Heat treated	36 ~ 37 HRC

4.8.2 Tensile Test:

Tensile strength is an important parameter for gauging the soundness of the material under load. Figure 4.12 show the photograph of the test specimen of heat treated material. Tensile test was carried out using universal testing machine with 300 KN loading while maintaining the cross head speed at 0.03 mm/min.

Figure 4.12: Photograph of Tensile Test Specimen (Heat Treated)

Table 4.3 summarizes ultimate tensile strength, yield strength and elongation of the test specimen.

Table 4.3: Material Tensile Strength

Tensile strength (MPa)	Yield strength (MPa)	Elongation (50mm gauge length)
905	633	12%

4.8.3 Ultrasonic Examination:

Ultrasonic examination of the runner blade was carried out to analyze the casting behaviour. Results of the ultrasonic test are shown in Table 4.4

Table 4.4: Ultrasonic Testing of Runner Blade

NDT REPORT Ultrasonic Examination						
Surface condition : Final Machine				Examination on : Casting		
Specifications : Sa-609				Equipment : USK-7		
Calibration : DGS-Scale				Method : Pulse Echo		
Technique : Normal Beam				Range : 250mm , 500mm		
Probes : Normal B2SN				Frequency : 2 MHz		
Couplant : Oil				Suppression : No		
S.NO	TOTAL QTY	TEST VOLUME %	TESTED QTY	DIMENSION	MATERIAL	RESULTS
1	01	100	01	AS PER DRG	A743	1
GENERAL : FINE GRAIN STRUCTURE				RESULT : ACCEPTED		

CHAPTER 5

5 STRESS ANALYSIS

5.1 Introduction

Structural stability of turbine blades is very important during operations in the hydro-power plants. As such it is very necessary that all the mechanical equipments especially turbine blades should conform to the stability criteria from strength point of view.

Before dynamic analysis, blades of all the five cases have to be checked for the structural stability for the maximum pressure loading conditions. In this chapter, stress analysis has been carried out on the runner blades. As described in Chapter-3, different blade profiles were developed in Pro-E / Creo with the help of coordinate points on hub, shroud, leading and trailing edges. These blade profiles were classified as case-A, case-B, case-C, case-D and case-E.

Physical properties of the blade material ASTM A743 grade CA6NM martensitic stainless steel [64] are as appended below;

Modulus of elasticity E = 2.0 x 10^{11} Pa (N/m^2)

Density = 7710 Kg/m^3.

Mechanical properties:

Tensile strength ≥ 830 MPa

Yield strength ≥ 690 MPa

The technical characteristics of the analyzed turbine are:

- runner diameter, D = 4240 mm
- nominal speed n = 107 rpm
- net head H = 6.7 m
- maximal power for net head Pmax = 4.6 MW

5.2 Static analysis of the blade

Static analysis study on the original blade (i.e. case-A) was carried out in ANSYS. In this procedure, model i.e. geometry of the blade was first imported in ANSYS in iges format from Pro-E / Creo. As the blade cannot be generated as a surface with constant thickness, for finite element analysis, only solid mesh (tetrahedral solid elements) can be used. Structural Solid Element SOLID186 was used for the analysis.

For static structural analysis loading, fixed type constraints applied to the area on hub side, which impose 0 value for the translations and rotations. Blade meshing and boundary condition is as shown in Figure 5.1. For constant head of 6.7m, total static pressure of 165,000 Pa as uniformly distributed load have been applied on the upper side of blade profile (pressure side).

Static analysis was performed after applying all the loading, constraints and boundary conditions to find the results.

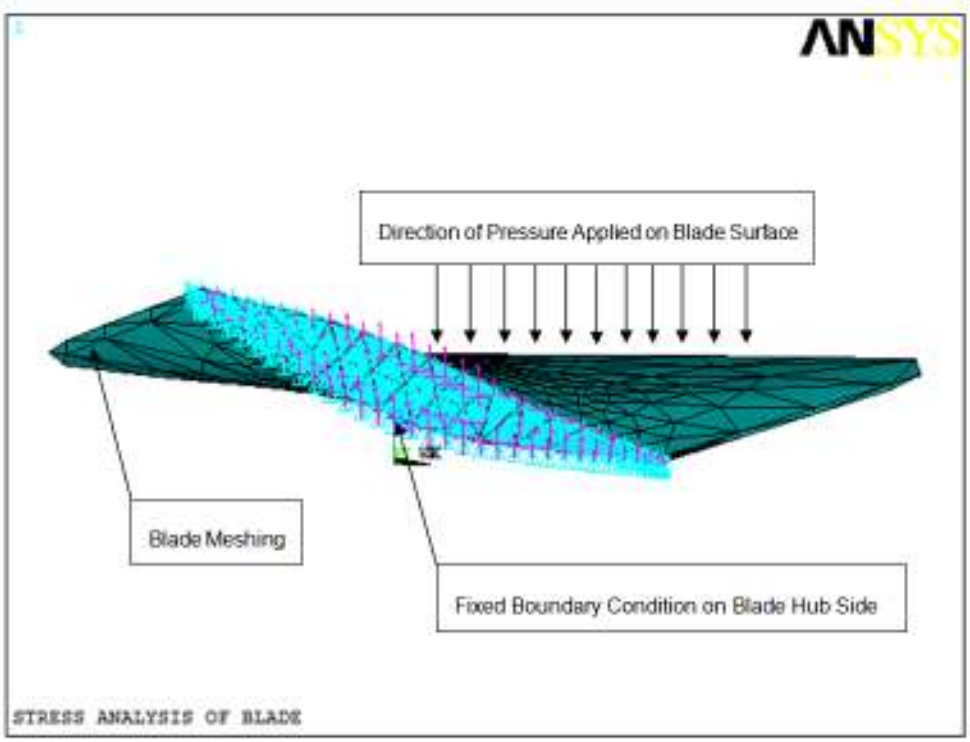

Figure 5.1: Blade Meshing and Boundary Condition

Results of the analysis were plotted as shown in the Figure 5.2 for Von Mises stresses and displacement of nodal solution for case-A. Figure 5.3 shows the

Von Mises stresses and displacement of element solution for case-A. Maximum stress value obtained for case-A is 0.89 x 10^8 Pa or 89.00 MPa.

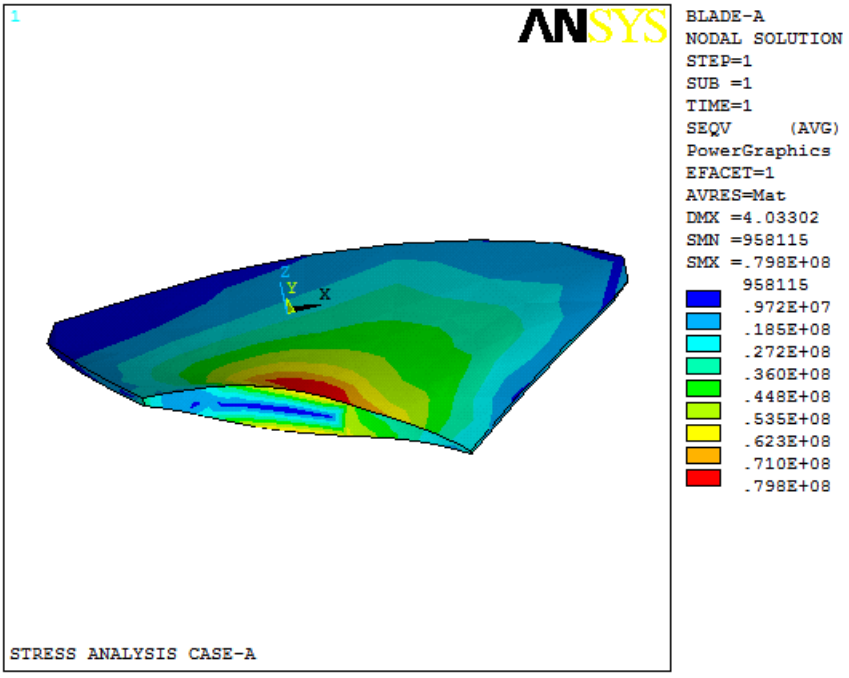

Figure 5.2: The Von Mises stress plot – Nodal Solution (case-A)

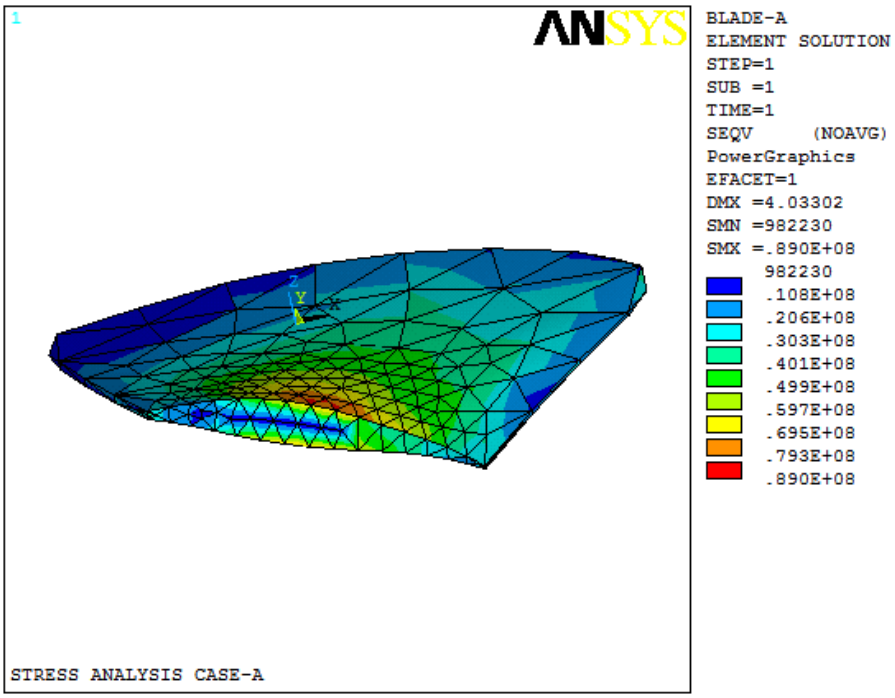

Figure 5.3: The Von Mises stress plot – Element Solution (case-A)

5.3 Static Analysis of the Developed Blades

Since blades with profiles case-B, case-C, case-D and case-E, have different surface areas and profile, accordingly there will be different behaviour on stresses. Static analysis study on these blades has been carried out in ANSYS similarly as carried out in the previous section.

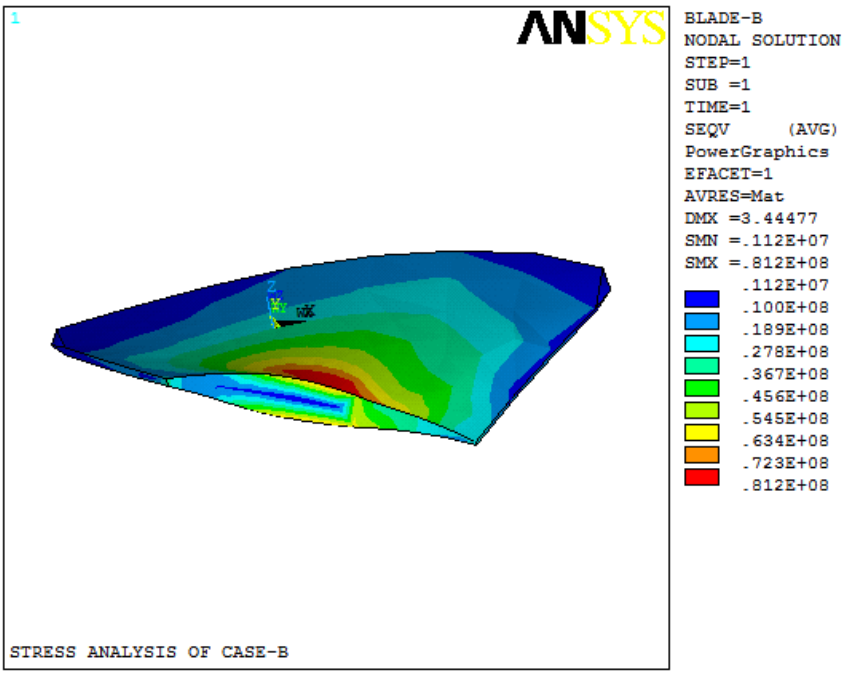

Figure 5.4: The Von Mises stress plot – Nodal Solution (case-B)

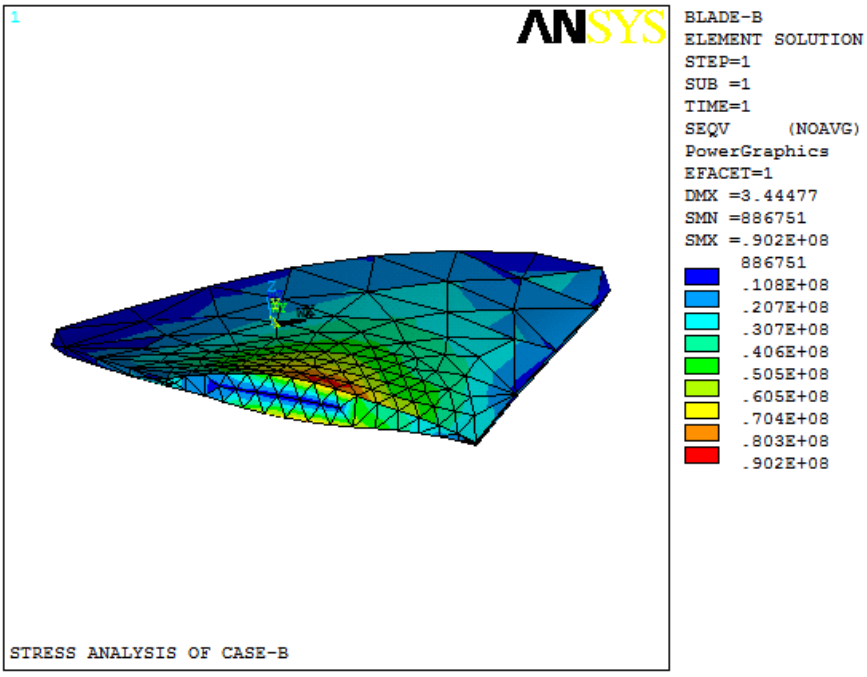

Figure 5.5: The Von Mises stress plot – Element Solution (case-B)

Figure 5.4 shows the Von Mises stresses and displacement of nodal solution for case-B, whereas Figure 5.5 indicates the Von Mises stresses and displacement of element solution for case-B. Maximum stress value obtained for case-B is 0.902 x 10^8 Pa or 90.20 MPa.

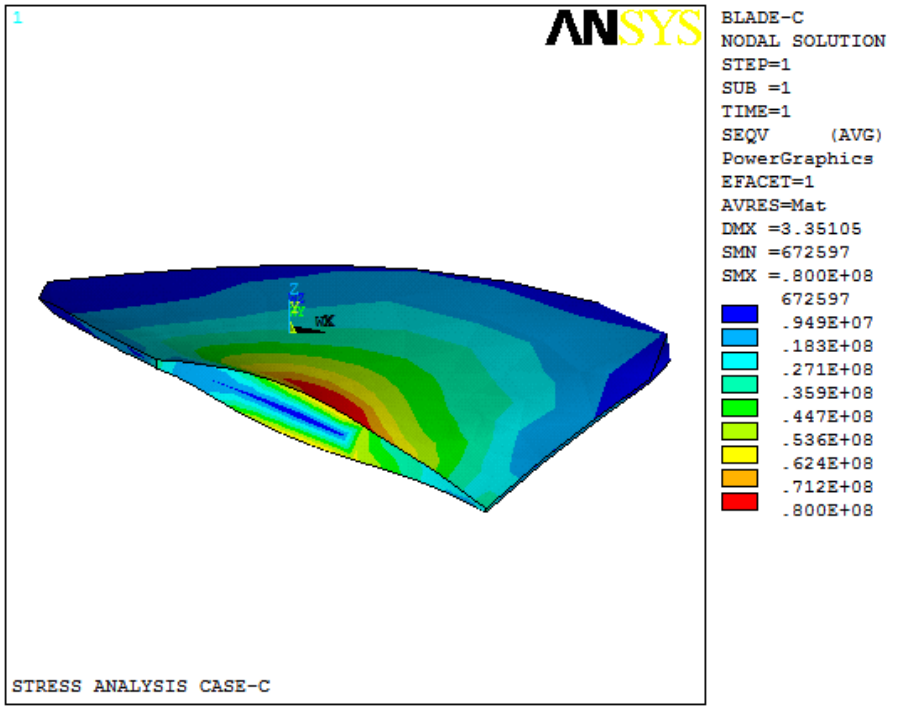

Figure 5.6: The Von Mises stress plot – Nodal Solution (case-C)

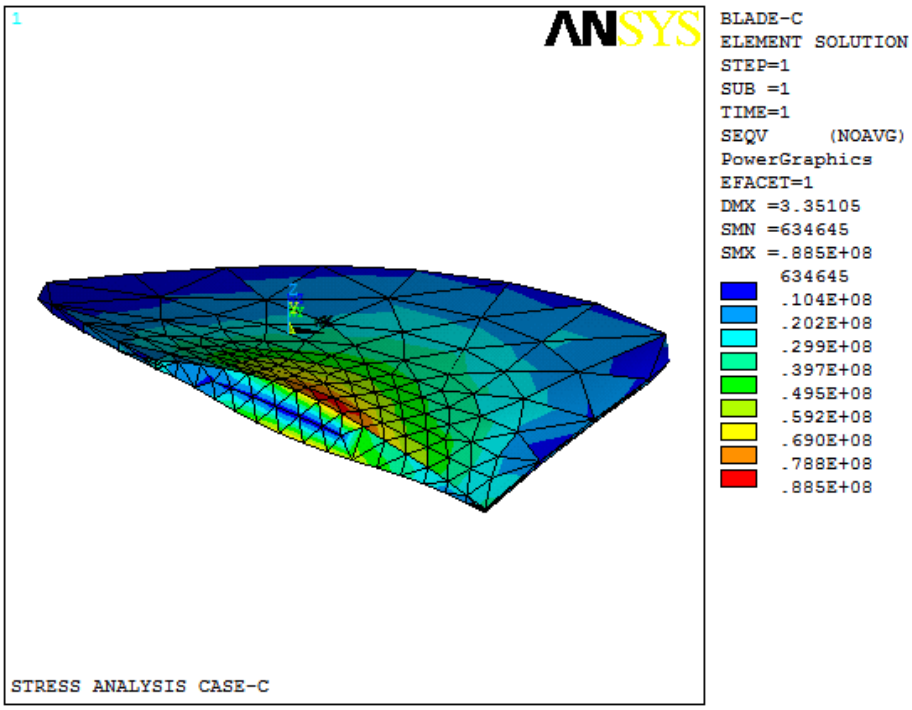

Figure 5.7: The Von Mises stress plot – Element Solution (case-C)

Figure 5.6 shows the Von Mises stresses and displacement of nodal solution for case-C, whereas Figure 5.7 indicates the Von Mises stresses and displacement of element solution for case-C. Maximum stress value obtained for case-C is 0.885 x 10^8 Pa or 88.50 MPa.

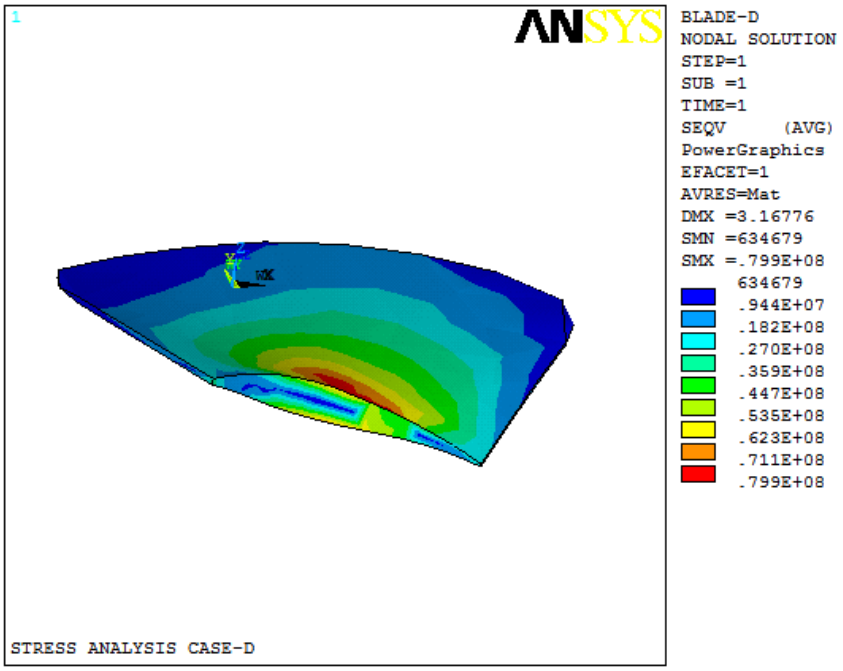

Figure 5.8: The Von Mises stress plot – Nodal Solution (case-D)

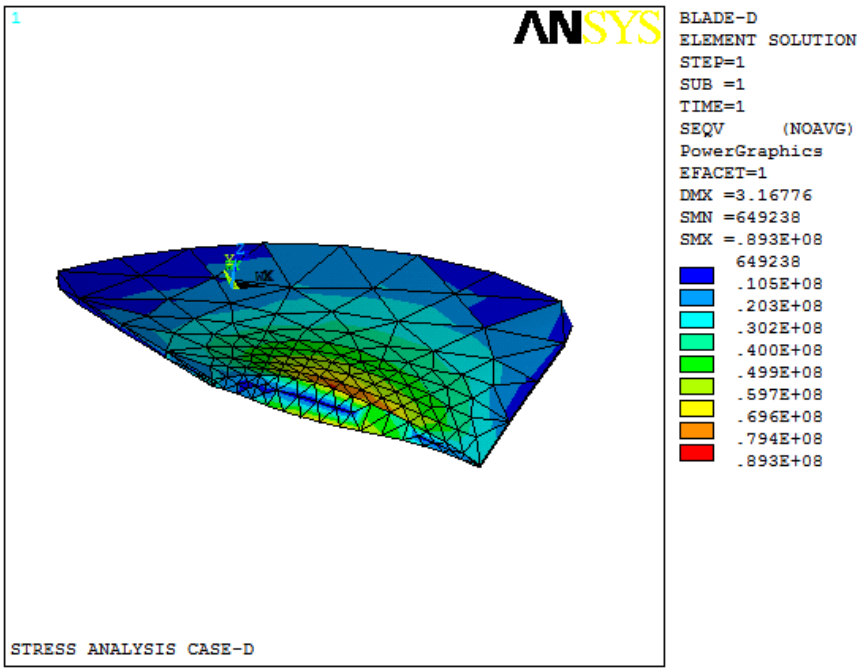

Figure 5.9: The Von Mises stress plot – Element Solution (case-D)

Figure 5.8 shows the Von Mises stresses and displacement of nodal solution for case-D, whereas Figure 5.9 indicates the Von Mises stresses and displacement of element solution for case-D. Maximum stress value obtained for case-D is 0.893 x 10^8 Pa or 89.30 MPa.

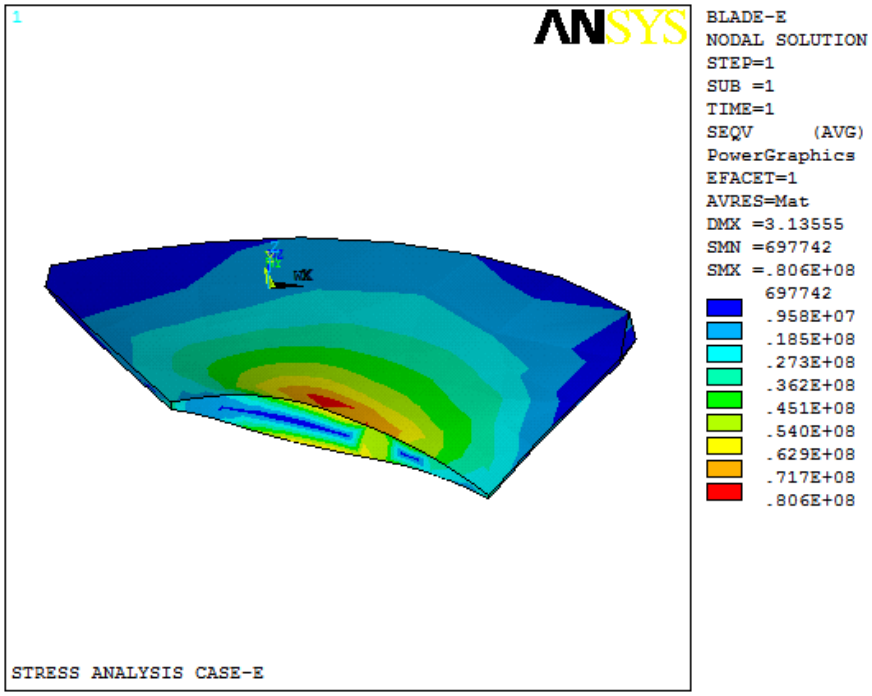

Figure 5.10: The Von Mises stress plot – Nodal Solution (case-E)

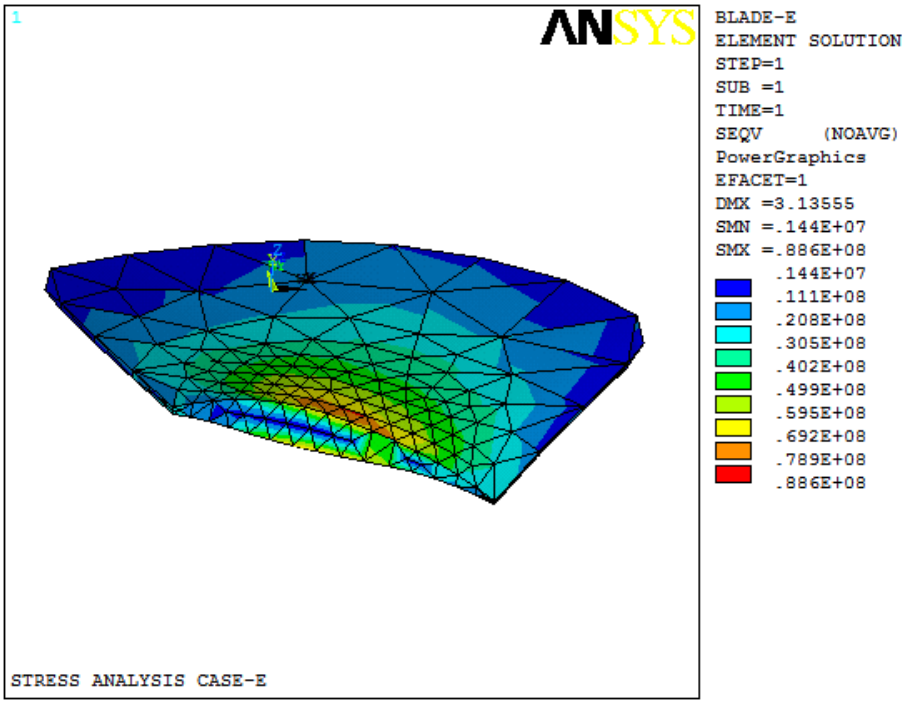

Figure 5.11: The Von Mises stress plot – Element Solution (case-E)

Figure 5.10 shows the Von Mises stresses and displacement of nodal solution for case-E, whereas Figure 5.11 indicates the Von Mises stresses and displacement of element solution for case-E. Maximum stress value obtained for case-E is 0.886 x 10^8 Pa or 88.60 MPa.

Result of maximum stresses and displacement of the static analysis carried out on all the five different blade profiles are shown in the Table 5.1.

Table 5.1 Results of static analysis.

Blade Profiles	Case-A	Case-B	Case-C	Case-D	Case-E
Pressure (Pa)	165000	165000	165000	165000	165000
Von Mises Stress (MPa) Element Solution	89.0	90.2	88.5	89.3	88.6
Von Mises Stress (MPa) Nodal Solution	79.8	81.2	80.0	79.9	80.6
Displacement Maximum (mm)	4.03	3.44	3.35	3.17	3.14

It is evident from the results shown that stresses produced under static load conditions and pressure are less than the ultimate tensile stress of the blade material at fixed boundary condition. Hence all the blade profile shapes are safe enough and blade models are statically stable against applied pressure loading.

Furthermore, blades were also analysed for pressure loading on different flow conditions as indicated in the table 5.2 for case-A. Whereas other blade profiles (i.e. case-B, case-C, case-D and case-E) were also statically analysed for pressure loading on different flow rates.

Table 5.2 Result of static analysis on different discharge conditions (case-A)

S.No	Discharge (m3/s)	Total Pressure (Pa)	Von Mises Maximum Stress (MPa)	Maximum Displacement (mm)
1	34.26	102,944	55.6	2.51
2	37.38	103,504	55.9	2.52
3	40.49	104,112	56.2	2.54
4	43.89	104,831	56.6	2.56
5	47.29	105,609	57.0	2.58
6	50.69	106,444	57.4	2.60
7	54.37	107,414	58.0	2.63
8	58.19	108,492	58.6	2.65
9	62.16	109,691	59.2	2.68
10	66.4	111,058	59.9	2.71
11	70.65	112,518	60.7	2.75
12	75.46	114,281	61.7	2.80
13	80.7	116,333	62.8	2.84
14	86.08	118,584	64.0	2.89

Results shown in the table 5.2 for case-A with pressure loading on different flow rate conditions indicate that the blade profile is stable in bending condition and displacements are within allowable limits.

Stress analysis results for case-B, case-C, case-D and case-E blade profiles are shown in appendix-B, which show structural stability of the blade profiles under static loading.

6 CFD ANALYSIS

6.1 Introduction

Computational Fluid Dynamics (CFD) is one of the branches of fluid mechanics that uses numerical methods to solve and analyze problems that involve fluid flows [29].

Computers are used to perform the millions of calculations required to simulate the interaction of fluids with the complex surfaces used in engineering. More accurate codes that can accurately and quickly simulate even complex scenarios such as supersonic or turbulent flows are an ongoing area of research [35].

CFD provides a qualitative as well as quantitative prediction of fluid flows by means of mathematical modelling (partial differential equations) and numerical methods (discretization and solution techniques). Computational Fluid Dynamics (CFD) is computer-based simulation to analyse systems involving fluid flow, heat transfer and associated phenomena [57]. A numerical model is first constructed using a set of mathematical equations that describe the flow. These equations are then solved using a computer programme in order to obtain the flow variables throughout the flow domain

6.2 CFD of turbine runner blade

The experimental approach of evaluating the performance of Kaplan turbine is costly as well as time consuming. Conversely CFD approach is faster and large amount of results can be produced at virtually no added cost.

Computational fluid dynamics study has been carried out using ANSYS [58] on the original geometry and results obtained were compared to validate with the operational / experimental data as illustrated in next sections.

6.2.1 Mesh Generation

For mesh generation, flow domain has to be divided in small cells. Its distribution locates the flow variables. These variable gradients are accurately calculated on the fine mesh.

A fine mesh has particular importance in the regions where large variations are expected in the flow are expected. It requires more computational power and time and mesh size is optimised by performing mesh-independence study. It starts from coarse mesh, until it refines by the time simulation results are not affected by doing any further refinement. A block topology for structured mesh is as shown in Figure 6.1

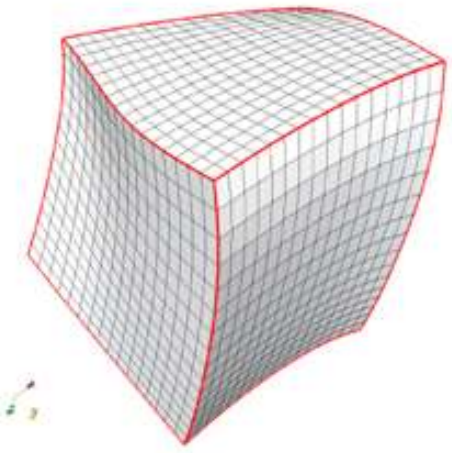

Figure 6.1: Block topology for structured mesh

3D blade runner geometry developed as shown in Figure 6.2 was used as an input to work in the ICEM. Initial topology was prepared for block structured hexahedral mesh. Geometry repairs were also carried for hub, shroud, blades, shaft and periodic surfaces.

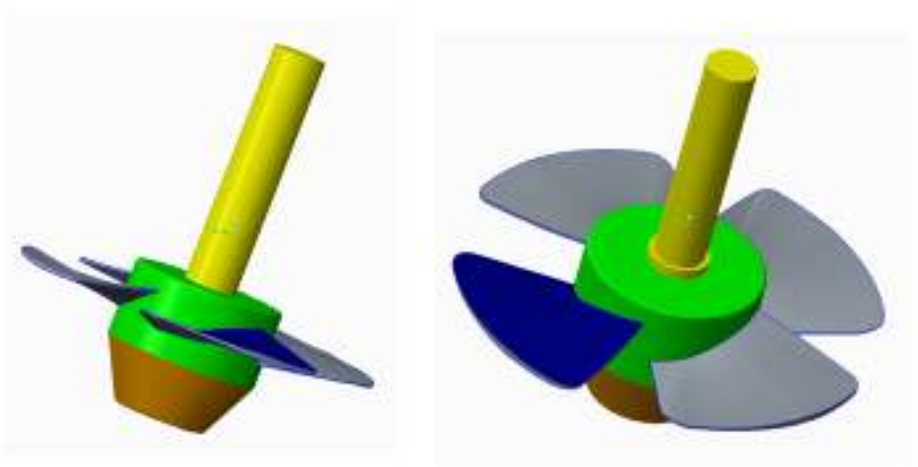

Figure 6.2: Runner blade model

Geometry was associated to blocking and then initial meshing was generated at 90^0 section containing one blade as shown in Figure 6.3. The geometry was meshed with tetrahedral cells of defined global size. Periodic surfaces were generated for the estimation of the effect of other three blades. For CFD analysis, turbulence model k-epsilon was used, as it is high Reynolds number model.

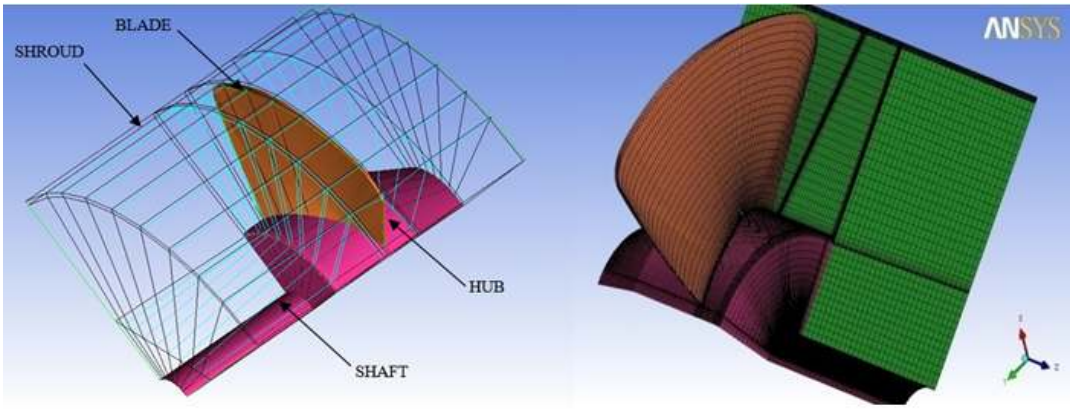

Figure 6.**3**: Topology and meshing of the blade assembly

6.2.2 Mesh independence study:

Mesh independence study is very important for optimising the mesh size required for CFD analysis. This independence study was done for the original blade-A with different meshing i.e. Mesh-A, Mesh-B, Mesh-C, Mesh-D, Mesh-E and Mesh-F. It was done through number of simulations with various meshing from coarse to fine mesh. From this study, global mesh size was determined.

Mesh optimization data taken for the study is shown in the Table 6.1. Whereas result output of the mesh optimization is elaborated numerically in Table 6.2 and graphically represented in Figure 6.4.

Table 6.1: Meshing data for CFD analysis

Mesh No.	Stream wise points	Span wise points	Passage	Tip	Tip clearance	Y plus	Total nodes
Mesh A	100	40	40	7	5	20	184000
Mesh B	100	50	40	7	5	20	224000
Mesh C	100	50	50	7	7	10	224000
Mesh D	100	60	50	7	7	1	264000
Mesh E	100	60	60	7	11	1	264000
Mesh F	125	60	60	9	13	1	330000

Table 6.2: Mesh optimization result

S.No	Discharge (m3/sec)	Experimental Data (MW)	Mesh optimization results (MW)					
			Mesh A	Mesh B	Mesh C	Mesh D	Mesh E	Mesh F
1	34.26	2	1.2	1.25	1.4	1.7	1.95	1.97
2	40.49	2.4	1.6	1.7	1.9	2.2	2.37	2.38
3	45.59	2.7	2.3	2.4	2.4	2.7	2.9	2.9
4	50.69	3	3	3.05	3.3	3.4	3.5	3.5
5	60.17	3.5	3.1	3.2	3.4	3.5	3.7	3.7
6	70.65	4	3.2	3.4	3.6	3.75	3.9	3.95
7	83.39	4.5	3.9	4.1	4.15	4.25	4.35	4.35
8	86.08	4.6	4.1	4.2	4.25	4.4	4.55	4.6

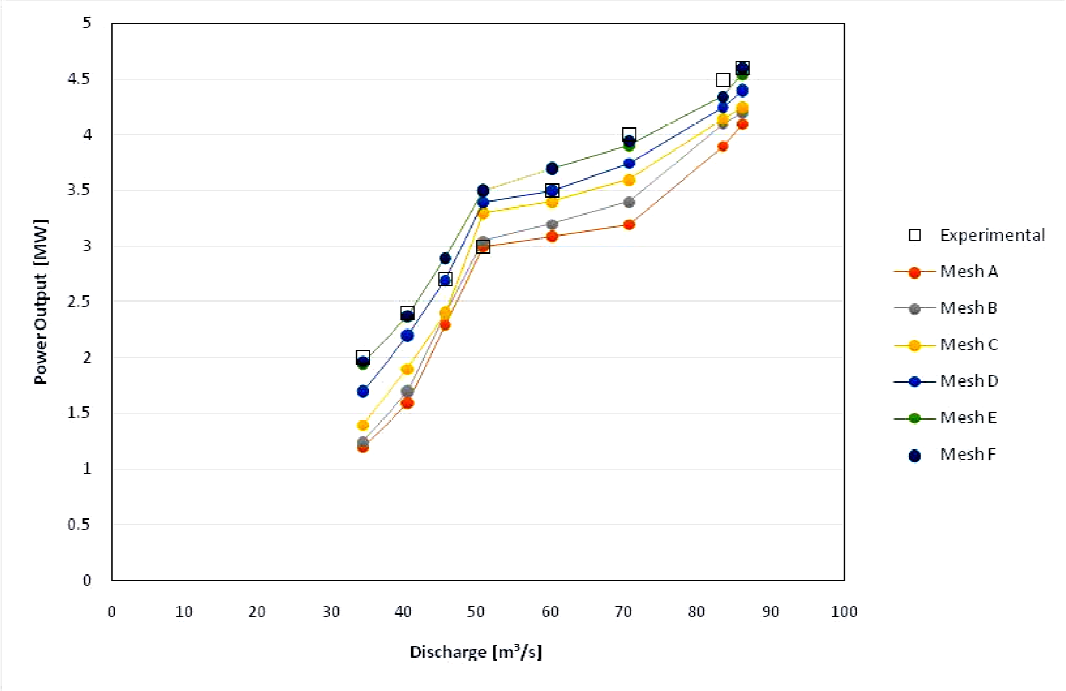

Figure 6.4: Meshing data for CFD analysis

6.2.3 Boundary Conditions of Developed Runner Geometry:

At inlet, total pressure was taken as Inlet boundary condition, whereas at outlet boundary volumetric flow rate was imposed as outlet boundary condition. Stationary wall boundary condition was given to the shroud i.e. outer casing. Blades and hub were given the rotating boundary conditions, while other surfaces were taken as periodic boundary conditions.

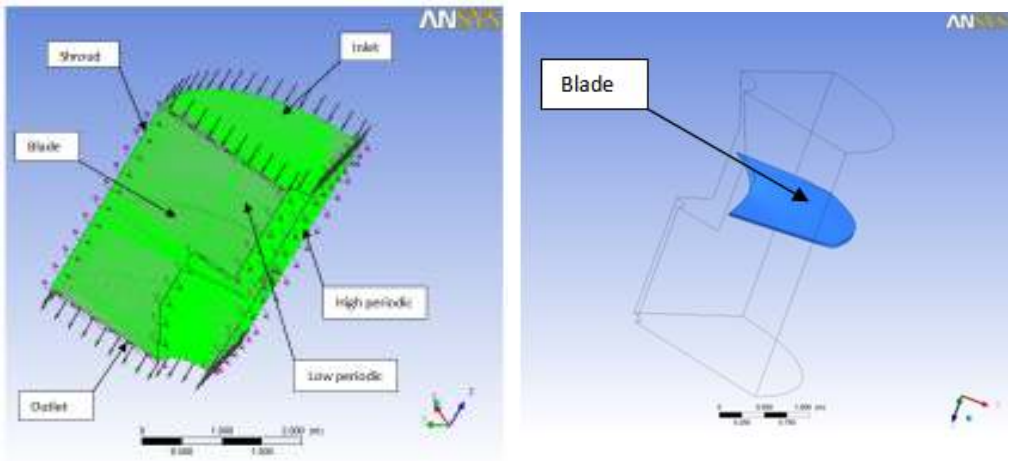

Figure 6.5: Boundary Conditions of Developed Runner Geometry

6.3 Validation of the CFD model

After CFD analysis it becomes very important to validate the results achieved. Validation is required for the assessment of the accuracy of computational model. Validation is achieved by comparing CFD results with available experimental data [59].

CFD analysis have been carried out on the original blade geometry at different flow rate conditions. Experimental / operational data was taken from the site of the hydro-power turbine unit located at Nandipur, Hydro Power Plant, near Gujranwala, Pakistan.

Experimental / operational data and CFD results obtained from the analysis carried on the original blade assembly i.e. case-A are tabulated in Table 6.3.

Table 6.3: Experimental data/CFD result of original assembly

S.NO	DISCHARGE (m^3/sec)	EXPERIMENTAL LOAD DATA (MW)	CFD RESULTS – Case A LOAD DATA (MW)
1	34.26	2.0	1.8
2	37.38	2.2	2.1
3	40.49	2.4	2.2
4	43.89	2.6	2.4
5	47.29	2.8	2.6
6	50.69	3	2.9
7	54.37	3.2	3.1
8	58.19	3.4	3.2
9	62.16	3.6	3.4
10	66.4	3.8	3.7
11	70.65	4	3.9
12	75.46	4.2	4.3
13	80.7	4.4	4.3
14	86.08	4.6	4.5

To compare the closeness of CFD simulation results to the experimental data, two measures, the percentage root mean square error and the percentage mean absolute error are used.

$$\%RMSE = \sqrt{\frac{\Sigma\left(P_{exp} - P_{cfd}\right)^2}{n}}\ x\ \frac{100\ .n}{\Sigma P_{cfd}}$$

$$\%MAE = \frac{\Sigma\left(P_{exp} - P_{cfd}\right)}{\Sigma P_{cfd}}\ x\ 100$$

Where P_{exp} is the experimental data, P_{cfd} is the CFD simulation result data and n is the number of operations.

The errors of the CFD simulation results with the experimental ones are found as 4.7% and 4% respectively. It shows that the CFD simulation results are in the sufficient agreement with experimental data and therefore validating the results.

Comparison between the experimental data and CFD results have been graphically represented in Figure 6.6. From results comparison, it is evident that power output of the turbine is close enough to be validated.

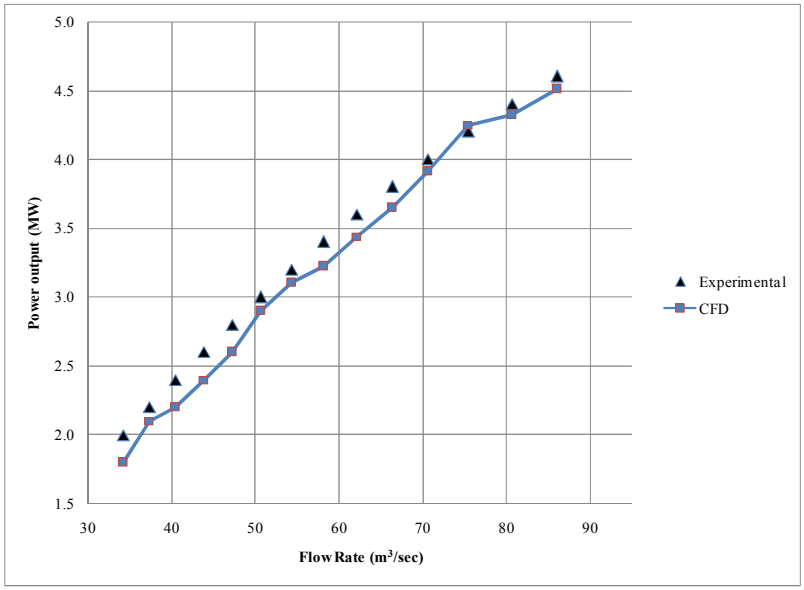

Figure 6.6: Comparison of experimental and CFD data

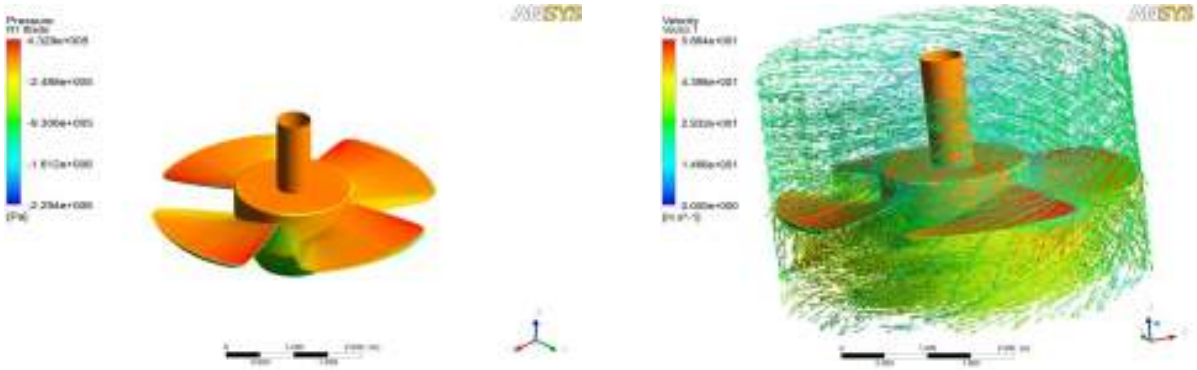

Figure 6.7: Pressure distribution and velocity streamlines on blades

Figure 6.7 shows the pressure distribution and velocity behaviour on the turbine blades. Water energy in terms of pressure is higher before striking the blade surface and goes on decreasing as energy is delivered by the water to do the work on turbine causing the blades to rotate.

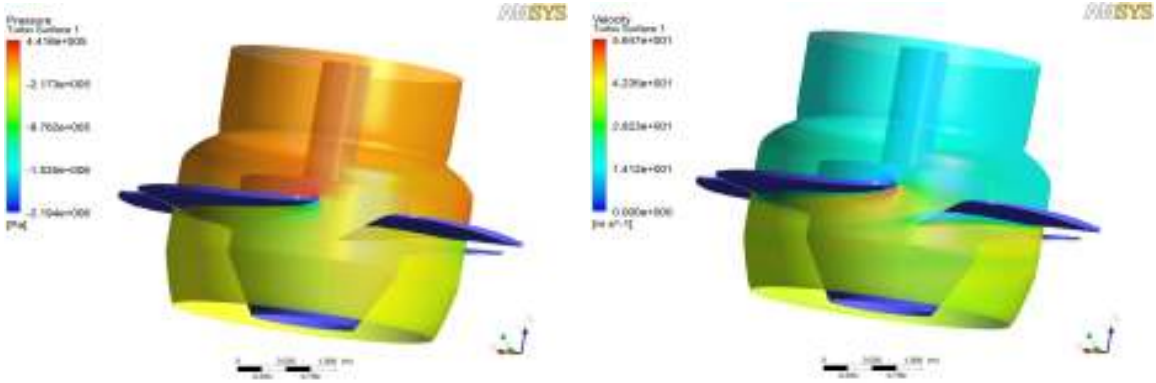

Figure 6.8: Pressure distribution and velocity streamlines on 50% span

Figure 6.8 shows the pressure distribution and flow velocity vectors on the blades assembly at 50% span.

Figure 6.9, Figure 6.10, Figure 6.11 and Figure 6.12 show the distribution of pressure as well as flow velocity vectors at the blades on 25%, 50%, 75% and 97% span respectively.

Flow visualization on the blades at different spans resulted from CFD simulations is shown in the following figures. It is obvious that flow is

streamline along the blade at various spans. There are no dead zones in the flow and also no major recirculation is found in these visualizations, which proves the validity and accuracy of CFD results.

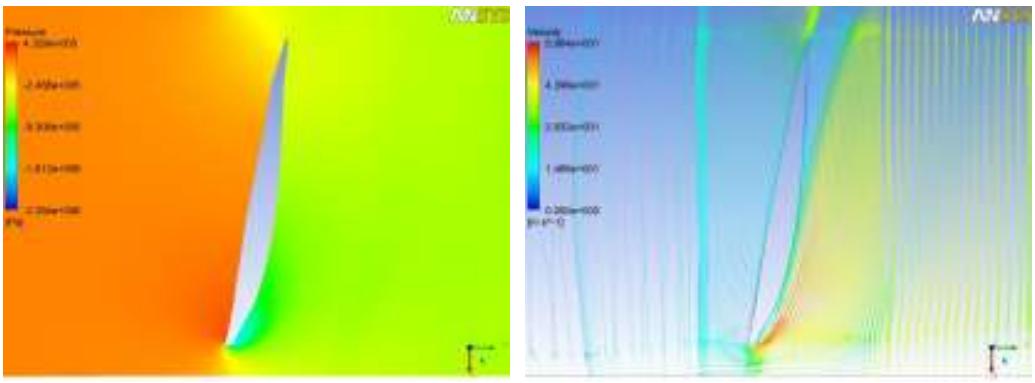

Figure 6-9: Pressure contours and velocity vectors on 25 % span

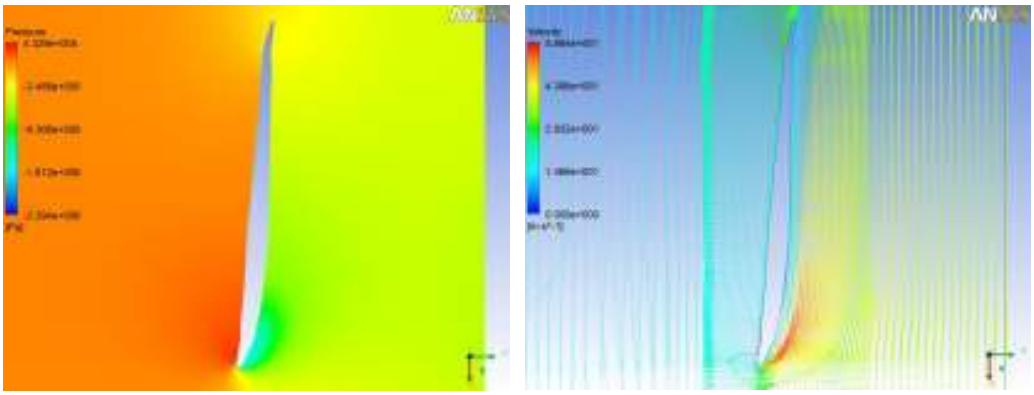

Figure 6-10: Pressure contours and velocity vectors on 50 % span

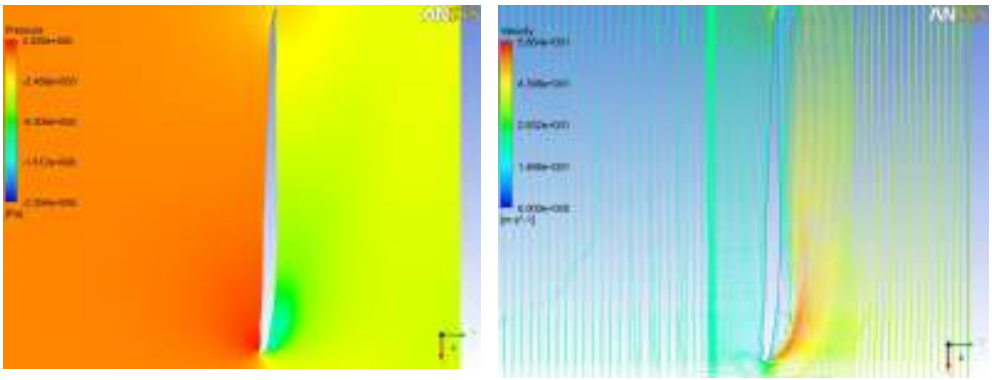

Figure 6-11: Pressure contours and velocity vectors on 75 % span

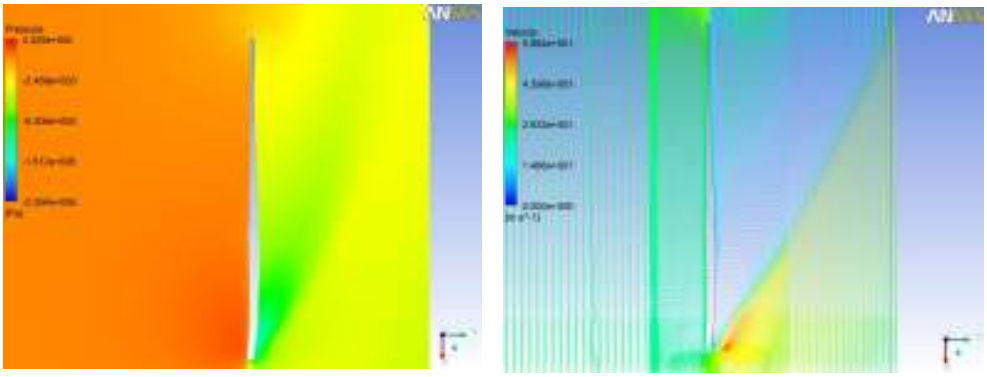

Figure 6-12: Pressure contours and velocity vectors on 97 % span

6.4 Blade profile optimization

To achieve the improved design characteristics and to optimise the blade profile, blade profile geometry was modelled and developed for four different cases i-e case-B, case-C, case-D and case-E at four different positions / inclinations on hub side.

These blade models were developed in Pro-E / Creo. Case-B and case-C developments were made at a position of angle 16.12^0 and 18.12^0 respectively. Whereas other two developments case-D and case-E were made at a position of angle 12.12^0 and 10.12^0 respectively. An average increment of 2^0 was considered for the angular displacement in clockwise and anticlockwise direction. CFD analysis was carried on the four different blade geometries consideration the same topology and boundary conditions taken in the earlier analysis.

From graphical representation shown in the figure, it is clearly indicated that CFD analysis on the developed blade profiles have improved the turbine power output. Results comparison have shown that blades used in the assembly for case-E have improved the power output of the turbine.

Table 6.4: Experimental data / CFD results of all blade assemblies

S.NO	DISCHARGE (m^3/sec)	EXPERIMENTAL DATA (MW)	CFD RESULTS – LOAD DATA (MW)				
			Case-A	Case-B	Case-C	Case-D	Case-E
1	34.26	2.0	1.8	1.59	1.40	2.00	2.11
2	37.38	2.2	2.1	1.87	1.75	2.33	2.45
3	40.49	2.4	2.2	2.15	1.98	2.58	2.66
4	43.89	2.6	2.4	2.19	2.00	2.65	2.77
5	47.29	2.8	2.6	2.41	2.28	2.83	2.91
6	50.69	3	2.9	2.73	2.59	3.12	3.32
7	54.37	3.2	3.1	2.95	2.80	3.41	3.48
8	58.19	3.4	3.2	3.02	2.84	3.44	3.55
9	62.16	3.6	3.4	3.20	3.05	3.65	3.77
10	66.4	3.8	3.7	3.48	3.35	3.90	4.04
11	70.65	4	3.9	3.70	3.51	4.11	4.21
12	75.46	4.2	4.3	4.00	3.81	4.46	4.58
13	80.7	4.4	4.3	4.10	3.92	4.54	4.70
14	86.08	4.6	4.5	4.28	4.10	4.74	4.85

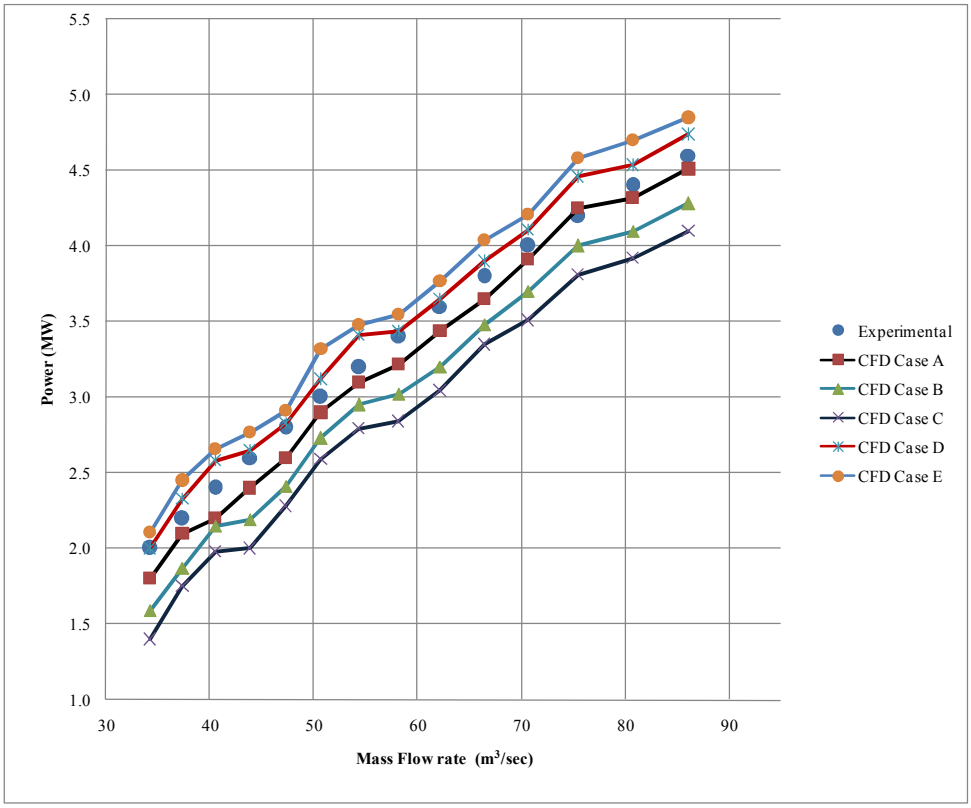

Figure 6.13: Experimental data and CFD results for all cases

Turbine blades have two sides, top one is pressure side with high pressure and the bottom side is suction side with low pressure. This pressure difference causes the blades to rotate. This pressure difference is very important and depends on the blade profiles. Optimum design of blade profiles using latest computational techniques can lead to the improvement in turbine power output.

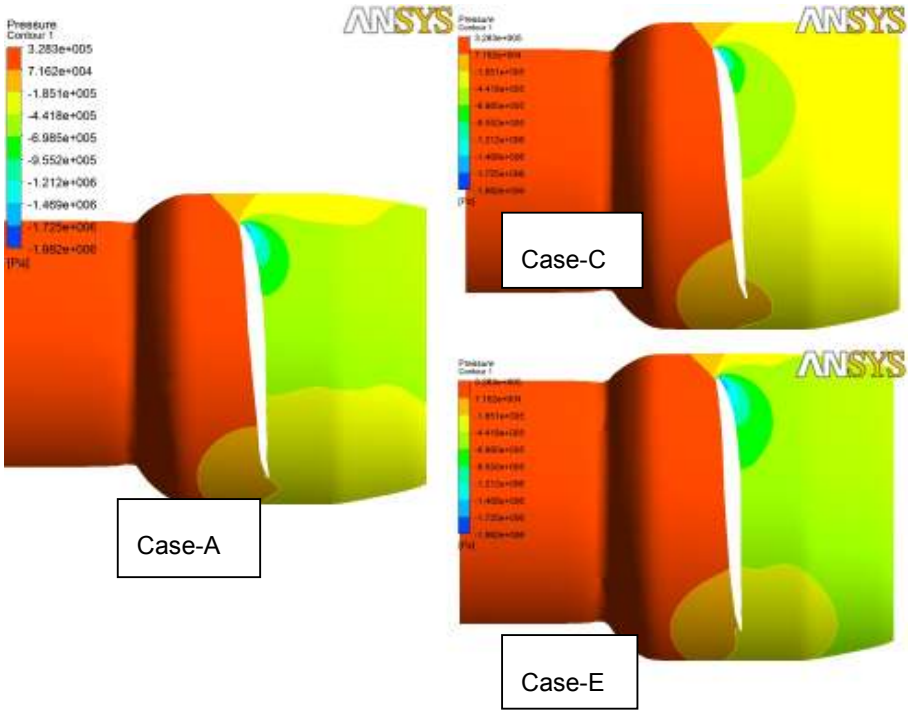

Figure 6.14: Pressure contours at 50% span for case-A, case-C and case-E

In our study as shown in Figure 6.14, red colour indicates the high pressure side, whereas green and yellow colour indicates low pressure side. While comparing the colour scheme to predict the pressure difference, it is found that for case-A, pressure difference is comparatively intermediate, for case-C there is low pressure difference and for case-E, there is highest pressure difference.

6.5 Pressure Loadings

Figure 6.15 shows the pressure loading at blades on both sides on 25% span for case-A, case-C and case-E. Similarly Figure 6.16 and Figure 6.17 show the pressure loading at blades on both sides on 50% and 75% span for case-A, case-C and case-E respectively. High-pressure difference on pressure sides of

the blade causes high torque. Pressure and suction sides are as shown in Figure 6.15.

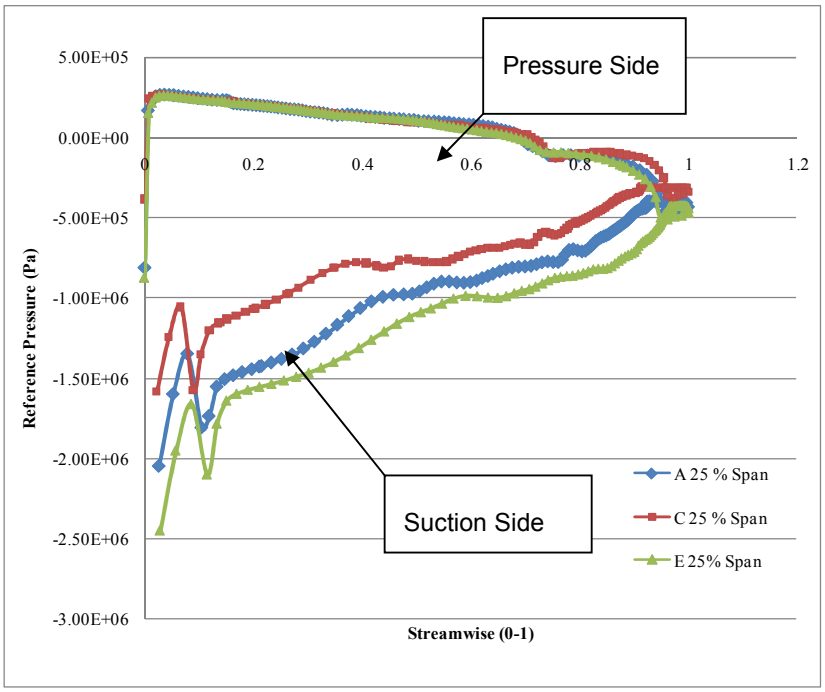

Figure 6.15: Pressure loading on blades at 25% span

Results have shown that blade profile developed for case-E is more efficient than blade profiles of case-C and case-A. High pressure difference resulted in case-E have shown improvement in the power output of the turbine.

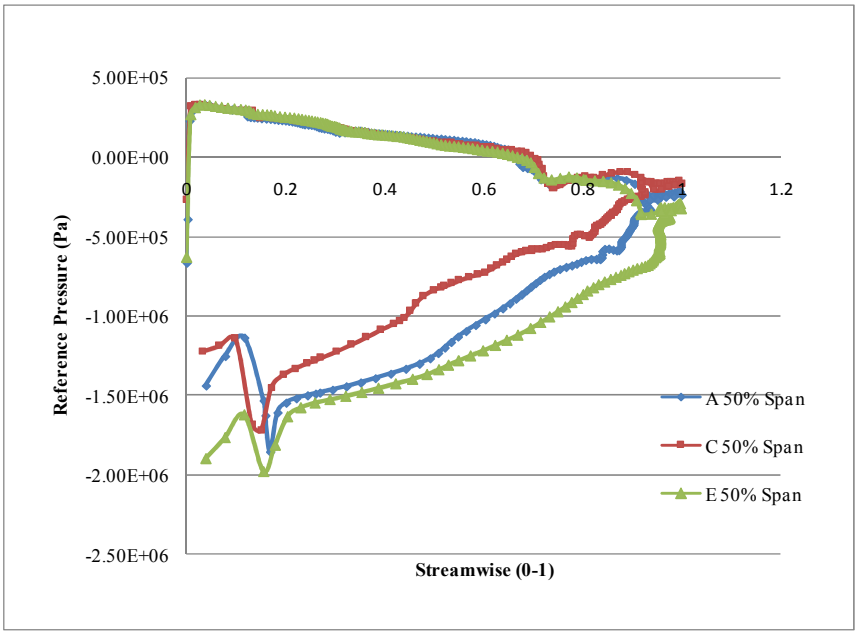

Figure 6.16: Pressure loading on blades at 50% span

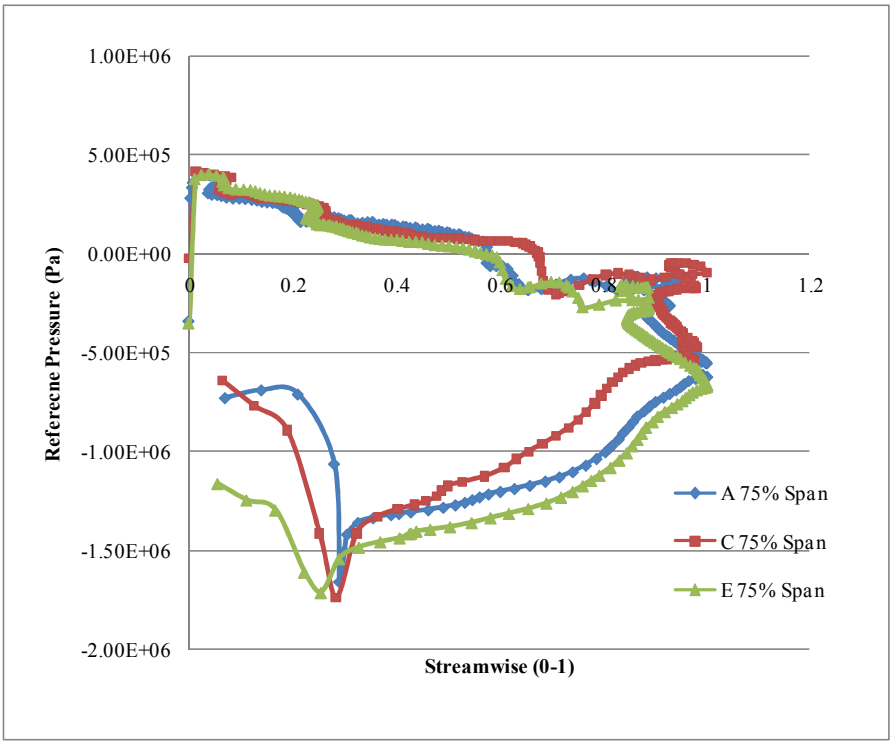

Figure 6.17: Pressure loading on blades at 75% span

CHAPTER 7

7 CONCLUSIONS AND RECOMMENDATIONS

7.1 Conclusions

An optimization methodology is developed for the design and development of Kaplan turbine runner blade using computational fluid dynamics tools. 3D CAD model of the original runner blade is generated from as-built physical measurements. Complex geometrical profile of the blade is developed using Pro-E/Creo for the purpose to analyse using CFD. Based on this geometry, four other modified profiles are developed to carry CFD analysis for optimum solution.

CFD simulation results are compared with the experimental site data to validate the CFD analysis. Results after comparison were found close enough to validate the CFD analysis.

The developed Kaplan turbine runner blade is manufactured locally in Pakistan and after successful completion three more blades were casted for a complete unit.

The developed methodology is applied for the Kaplan turbine runner blade design of an actual hydropower project. The project is a small hydropower plant named Nandi-pur HPP located in Gujranwala, Pakistan. Three units of 4.6MW each are installed in the hydropower plant. CFD results indicated an overall turbine efficiency of 84.3%.

Results of the research study carried out on the CAD model of original blade and modified blade profiles have shown improvement in the turbine power output, resulting in the power output increase from 4.6 MW to 4.85 MW (i.e 5.43% increase. The same improved output of 4.85MW have also been verified at site. It resulted an increase of around 6000 kwh units per day or 180,000 kwh per month, having financial impact of worth Rs. 1.8 million or 18,000 US Dollar (i.e. equivalent @ Rs. 100/- equal to one US Dollar) per month saving for 4.6 MW turbine unit.

Utilization of CFD approach in this research assisted in the cost reduction of model testing / prototype and also time saving, leading to the cost-effective measures and also the enhanced viability of hydropower development.

It is concluded that use of model testing or prototyping of a turbine can easily be avoided by replacing the use of CFD techniques for cost effectiveness. It is not worthy to carry expensive testing of turbines, as turbine blade designs vary with every site and location.

From the research work carried out, it is concluded that all types of hydro turbines and their components in comparison with varying flow conditions and flow behaviours can be optimized and developed for improved results.

7.2 Recommendations

In future research, CFD study can be conducted on the hydro-mechanical components of water turbines for improvement to obtain optimum solutions.

This study can be based on many aspects like component material behaviours, structural stability, economical measures, indigenization criteria, standardization in the design.

Furthermore, following recommendation can be addressed for future research work in the research field of hydro-power development in the developing countries;

- Study on the use of composite material as replacement to the conventionally used materials on blades for the cost effectiveness and better and better performance.

- To carry research for improvement in the turbine efficiencies depending on the blade tip clearance criteria using CFD techniques.

- To carry research work on the turbine balancing techniques using latest computational techniques.

- Research work in the area of hydraulic structures need more attention. Use of CFD can lead to improved and optimum design of hydraulic structures like gates, stoplogs, trashracks etc.

- To investigate the criteria for optimum design and development of penstock, bifurcation and expansion joints through dynamic analysis.

BIBLIOGRAPHY

[1] Kobayashi, H., “Micro Hydropower Generation: Its Potential and Expectations,” Renewable Energy Brightens Up the Local Community, pp. 42-53, 2007

[2] Paish, O., “Small hydro power : technology and current status”, Renewable and Sustainable Energy Reviews, Volume 6, No. 6, pp. 537-556, UK, 2002

[3] Demirbas, A. “Potential applications of renewable energy sources, biomass combustion problems in boiler power systems and combustion related environmental issues”, Progress in Energy and Combustion Science, 31, pp.171-192, 2005

[4] Gaius-obaseki T., “Hydropower opportunities in the water industry”, International Journal of Environmental Sciences, Volume 1, No 3, pp 392-402, 2010.

[5] Hammad, M., Aburas, R. and Abuzahra, B., “The potential of hydropower generation in Jordan: Micro hydropower analysis”, Energy Policy, pp. 523-530, 1994

[6] Maqsood, S. Qureshi., “Role of WAPDA in the development of hydel potential in Pakistan” Water and power development authority, August 2009

[7] Zhou, L., Wang, Z., Xiao, R., and Luo, Y., “Analysis of dynamic stresses in Kaplan turbine blades”, International Journal for Computer-Aided Engineering and Software Vol. 24 No. 8, pp. 753-762, 2007

[8] Swiderski J., J. Martin, “Practical Implementations of Computational Fluid Dynamics in the Design Practice - Virtual Hydraulic Laboratory”, Conference materials, Hydroforum, Poland, 2000

[9] Bennett K., and Swiderski, J., “Application of CFD Turbine Design for Small Hydro Elliott Falls, A Case Study”, Waterpower XII, Salt lake City, 2001

[10] Grekula, M., and Bark, G.O., “Experimental Study of Cavitations in a Kaplan Model Turbine”, Chalmers University of Technology, Sweden, 2001

[11] Laura A. Garrison and Richard K. Fisher, Jr, “Application of Biological Design Criteria and Computational Fluid Dynamics to Investigate Fish Survival in Kaplan Turbines”, Voith Siemens Hydro Power Generation, Inc.; Oak Ridge National Laboratory, USA, 2002

[12] Deschenes, C., Fraser, R., and Fau, J.P., “New Trends in Turbine Modelling and New Ways of Partnership”, Laval University Hydraulic Machinery Laboratory (LAMH), Canada, 2002

[13] Dragu, C., Soens, J., and Belmans, R., “Small-Scale Renewable Energy in The Next Century Market Hydro Plants - State of The Art and Applications”, ELECTA, Energy Institute, Belgium, 2003

[14] Jean-Louis Kueny, Rémi Lestriez , Assia Helali, Alain Demeulenaere, Charles Hirsch., “Optimal design of a small hydraulic turbine”, Brussels, Belgium, 2004

[15] Busea, C., and Jianu, B., “Optimization of axial hydraulic turbines runner blades using Hydrodynamic simulation techniques”, 6th International Conference on Hydraulic Machinery and Hydrodynamics, Timisoara, Romania, October 21 - 22, 2004

[16] Ferrando, L., Kueny, J.L., Avellan. F, Pedretti, C, and Tomas, L., “Surface Parameterization of a Francis Runner Turbine for Optimum Design”, 22nd IAHR Symposium on Hydraulic Machinery and Systems, June 29 – July 2, Sweden, 2004

[17] Tiaple1,Y., and Nontakaew, Y., “The Development of Bulb Turbine for Low Head Storage Using CFD Simulation”, The Joint International Conference on “Sustainable Energy and Environment (SEE)”, 1-019 (O), pp 49-52, Hua Hin, Thailand, 1-3 December 2004

[18] Barglazan, M., “About design optimization of cross-flow Hydraulic turbines”, Romania, 2005

[19] Oftebro, I., Lønning, A., “Pressure oscillations in Francis turbines”, Proc Inst Mech Engrs, Vol. 181, 1967

[20] Doerfler, P., “On the role of phase resonance in vibrations caused by blade passage in radial hydraulic turbo machines”, Proceedings of the 12th IAHR Symposium, Stirling, 27-30 August 1984

[21] Coutu, A., Velagandula, O., Nennemann, B., “Francis runner forced response technology”, Proceedings Waterpower XIV, Austin, Texas, USA, July 18-22, 2005

[22] Mather, J.S.B., Savidge, J., Fisher, M.J., “New observations on the tone generation in fans”, Journal of Sound and Vibrations, Vol. 16. 1971

[23] Tanaka, H., “Vibration behaviour and dynamic stress of runners of very high head reversible pump-turbines”, IAHR Symposium, special session, Belgrade, Yugoslavia, 1990

[24] Arndt, N., Acosta, A.J., Brennen, C.E., Caughey, T.K., “Rotor-Stator Interaction in a Diffuser Pump”, Journal of Turbo machinery, Vol. 111, July 1989

[25] Dring, R.P., Joslyn, H.D., Hardin, L.W., Wagner, J.H., “Turbine Rotor-Stator Interaction”, Journal of Engineering for Power, Vol. 104, October 1982

[26] Vu, T.C., Nennemann, B., G.D. Ciocan, M.S. Iliescu, O. Braun, F. Avellan, “Experimental study and unsteady simulation of the Flindt draft

tube rotating vortex rope", Proceedings Hydro 2004, Porto, Portugal, 18-21 October, 2004

[27] Kuntz, M., Menter, F., Garcin, H., Parkinson, E., Habertheurer, N., "Numerical investigation of turbo machinery performance of a pump-turbine", Proceedings of the 21st IAHR Symposium on Hydraulic Machinery and Systems, Lausanne, Switzerland, 9-12 September 2002

[28] Williams, A.A., and Simpson, R.G., "Application of computational fluid dynamics to the design of pico propeller turbines", Proceedings of the International Conference on Renewable Energy for Developing Countries - 2006

[29] Jingchun Wu, Shimmei, K., Tani, K. Niikura, K. and Sato, J., "CFD-Based Design Optimization for Hydro Turbines", Journal of Fluids Engineering, ASME, Vol. 129, pp.159-168, February 2007

[30] Cruz, A.G.B., Mesquita, A.L.A, and Blanco, C.J.C., "Minimum Pressure Coefficient Criterion Applied in Axial-Flow Hydraulic Turbines", Journal of the Brazil Society of Mechanical Science & Engineering, Vol. XXX, No. 1, pp.30-38, January-March 2008

[31] Keck, H. Michler, W. Weiss, T. and Sick, M., "Recent Developments in the Dynamic Analysis of Water Turbines", Proceedings of the 2nd IAHR International Meeting of the Workgroup on Cavitations and Dynamic Problems in Hydraulic Machinery and Systems, pp.9-20, Timisoara, Romania, October, 2007

[32] Risberg, S., Jonassen, M. and Jonassen, R., "Design of Francis turbine runners based on a surrogate model approach", International Journal of Hydropower & Dams - Volume Fifteen, Issue 5, 2008

[33] V.C. Campian, V.C, Frunzaverde, D., Nedelcu, D. Marginean, G. "Failure Analysis of A Kaplan Turbine Runner Blade" IAHR, 24th Symposium on Hydraulic Machinery and Systems October 27-31, FOZ DO IGUASSU, 2008

[34] ShuHong, L., Jie, S., ShangFeng, W., and YuLin, W., “Numerical simulation of pressure fluctuation in Kaplan turbine”, Science in China Press, vol. 51, No. 8, pp.1137-1148, August, 2008

[35] Prasad, V., Gahlot, V.K., and Krishnamachar., “CFD approach for design optimization and validation for axial flow hydraulic turbine”, Indian Journal of Engineering & Materials Sciences Vol. 16, pp. 229-236, August 2009

[36] Raabe I J, “Hydro Power- The design, use and function of hydro mechanical hydraulic and electrical equipment” (VDI-Verlag, GmbH, Dusseldorf), 1985

[37] Shukla, M. K., Jain, R., Prasad, V., and Shukla, S. N., “CFD analysis of 3-D flow for Francis turbine”, MIT, International Journal of Mechanical Engineering, Vol-1, No-2, pp 93-100, 2011

[38] Peng, G., Cao, S., Ishizuka, M., and Hayama, S., “Design optimization of axial flow hydraulic turbine runner” International Journal of Numerical Methods in Fluids, 39(6) pp 533-548, 2002

[39] Daniel, B., Romeo, R., and Sebastian M., “A numerical approach for the 3D flows in Kaplan turbine” Proceedings of the International Conference on CSHS03, Belgrade, pp. 29-36, 2003

[40] Liplej, A., “Optimization method for the design of axial hydraulic turbines”, Proceedings of the Institution of Mechanical Engineers, Journal of Power and Energy, Volume 218, No. 1, pp. 43-50, UK, 2004

[41] Guoyi Peng., “A practical combined computation method of mean through-flow for 3D inverse design of hydraulic turbomachinery blades”, Journal of Fluids Engineering, Volume-127, issue-6, pp 1183-1190, 2005

[42] Wu J, Shimmel K, Tani K, Niikura K & Sato J.,”CFD based design optimization for hydro turbines”, Journal of Fluid Engineering, Vol. 129 pp. 159-168, 2007

[43] Shukla, M., “CFD analysis of 3-D flow and its validation for Francis turbine”, M. Tech. Thesis, Maulana Azad National Institute of Technology, Bhopal, 2007

[44] Faizan, A., “Validation of CFD Analysis of Pump as Turbine”, M. Tech. Thesis, Maulana Azad National Institute of Technology, Bhopal, 2007

[45] Rao V S & Tripathi S K, Proc Nat Seminar on CFD-The 3rd Dimension in Flow Analysis & Thermal Design, Bhopal, India, pp 196-201, 2007

[46] Singh, P., and Nestmann., “Experimental optimization of a free vortex propeller runner for micro hydro application”, Journal of Experimental Thermal and Fluid Science Vol. 33, pp.991–1002, 2009

[47] Khare, R., Prasad, V., and Kumar, S., “Derivation of Global Parametric Performance of Mixed Flow Hydraulic Turbine Using CFD” Hydro Nepal: Journal of Water, Energy and Environment, Vol-7, pp 60-64, 2010.

[48] Helena, M.R., Mariana. S., “Hydrodynamic and performance of low power turbines: conception, modelling and experimental tests”, International Journal of energy and environment, Volume 1, No. 3, pp.431-444, Lisbon, Portugal, 2010

[49] Nicolle, J., Labbe, P., Gauthier, G., and Lussier, M., “Impact of blade geometry differences for the CFD performance analysis of existing turbines”, 25th IAHR Symposium on Hydraulic Machinery and Systems, 2010.

[50] Paik, N.C., Byeon, S.S., and Kim, Y.J., “Numerical optimization of an axial propeller runner for small-hydro power application”, 2010

[51] Sutikno, P., and Adam, I.K., “Design, Simulation and Experimental of the Very Low Head Turbine with Minimum Pressure and Free Vortex Criterions”, International Journal of Mechanical & Mechatronics Engineering IJMME-IJENS Vol. 11, No. 01, pp.9-15, 2011

[52] Thapa, B.S., Panthee, A., and Thapa, B., “Computational Methods in Research of Hydraulic Turbines”, International Journal of Advanced Renewable Energy Research, Vol. 1, No. 2, pp.1-4, 2012

[53] Santa, J.F., Blanco, J.A., Giraldo, J.E., and Toro, A., “Cavitations erosion of martensitic and austenitic stainless steel welded coatings”, 18th International Conference on Wear of Materials, Volume 271, No. 9-10, pp.1445-1453, Colombia, 2011

[54] Khurana, S., Navtej., and Singh, H., “Effect of cavitation on hydraulic turbines – A review”, International journal of Current Engineering and Technology, Vol-2, No-1, 2012.

[55] Santa, J.F., Baena, J.C., and Toro, A., “Slurry erosion of thermal spray coatings and stainless steels for hydraulic machinery”, Wear 263 pp 258–264, 2007

[56] Prasad, V., Khare, R., “CFD: An Effective Tool for Flow Simulation in Hydraulic Reaction Turbines”, International Journal of Engineering Research and Applications (IJERA), Volume 2, No. 4, pp.1029-1035, India, 2012

[57] Versteeg, H and Malalasekera, W., “An introduction to computational fluid dynamics”, 2nd Edition, Pearson Education Limited, England, 2007

[58] ANSYS 13.0 User’s manual guide ANSYS Inc. Southpointe Canonsburg PA 15317, USA, 2010

[59] Oberkampf, W.L., and Trucano, T.G., “Verification and validation in computational fluid dynamics”. Progress in Aerospace Sciences, 38, pp 209–272, 2002

[60] Lewis R I, “Turbo machinery Performance Analysis” Arnold, London, 1996

[61] Huang, H., Yan, Z., “Present situation and future prospect of hydropower in China”, Renewable and Sustainable Energy Reviews, Volume 13, pp. 1652–1656, China, 2009.

[62] Zaigham, N.A., Nayyer, Z.A., “Prospects of Renewable Energy Sources in Pakistan” , Proceedings of Renewable-Energy Technologies and Sustainable Development, Volume 4, pp. 65-86, Pakistan, 2005.

[63] Vu, T.C., Retieb S., “Accuracy Assessment Of Current CFD Tools To Predict Hydraulic Turbine Efficiency Hill Chart”, Proceedings of the 21st IAHR Symposium on Hydraulic Machinery and Systems, Lausanne, Switzerland, 9-12 September 2002

[64] Silva, B. L, Ferreira, J. L. A, and Araújo, J. A., “High-cycle notch sensitivity steel ASTM A743 CA6NM used in hydrogenator turbine components”, Frattura ed Integrita Strutturale, Vol. 14 pp 36-44, Brazil, 2010

[65] Coutu, A., Proulx, D., Coulson, S., Demers, A., “Dynamic Assessment of Hydraulic Turbines”, Proceedings of Hydro Vision 2004, Montreal, Quebec, Canada, August 16-20, 2004

APPENDIX-A

Table A-1: Coordinate points for hub and shroud side (case – B)

	Hub side – upper edge		
Point	X-axis (mm)	Y-axis (mm)	Z-axis (mm)
1	643	-1519	13
2	600	-1476	32
3	500	-1396	74
4	400	-1336	117
5	300	-1293	159
6	200	-1263	215
7	100	-1246	266
8	0	-1240	311
9	-100	-1246	348
10	-200	-1263	381
11	-300	-1293	409
12	-400	-1336	439
13	-457	-1368	456

	Hub side – lower edge		
Point	X-axis (mm)	Y-axis (mm)	Z-axis (mm)
1	643	-1519	0
2	600	-1476	6
3	500	-1396	21
4	400	-1336	36
5	300	-1293	50
6	200	-1263	68
7	100	-1246	94
8	0	-1240	131
9	-100	-1246	178
10	-200	-1263	238
11	-300	-1293	310
12	-400	-1336	383
13	-457	-1368	425

	Shroud side - upper edge		
Point	X-axis (mm)	Y-axis (mm)	Z-axis (mm)
1	-100	-2	287
2	-200	-10	284
3	-300	-21	281
4	-400	-38	280
5	-500	-60	280
6	-600	-87	282
7	-700	-119	287
8	-750	-140	290
9	-775	-158	292
10	-800	-185	296
11	-825	-229	301
12	0	0	291
13	100	-2	293
14	200	-10	295
15	300	-21	297
16	400	-38	298
17	500	-60	298
18	600	-87	298
19	700	-119	298
20	800	-157	296
21	900	-201	294
22	1000	-251	290
23	1100	-308	293
24	1200	-379	275
25	1250	-447	269
26	1270	-497	263
27	1281	-569	257

	Shroud side - lower edge		
Point	X-axis (mm)	Y-axis (mm)	Z-axis (mm)
1	-100	-2	215
2	-200	-10	217
3	-300	-21	218
4	-400	-38	222
5	-500	-60	224
6	-600	-87	226
7	-700	-119	236
8	-750	-140	245
9	-775	-158	249
10	-800	-185	261
11	-825	-229	271
12	0	0	223
13	100	-2	221
14	200	-10	224
15	300	-21	232
16	400	-38	236
17	500	-60	240
18	600	-87	244
19	700	-119	247
20	800	-157	249
21	900	-201	253
22	1000	-251	254
23	1100	-308	253
24	1200	-379	247
25	1250	-447	243
26	1270	-497	242
27	1281	-569	241

Table A-2: Coordinate points for leading and trailing side (case – B)

	Leading side – upper edge		
Point	X-axis (mm)	Y-axis (mm)	Z-axis (mm)
1	-837	-295	322
2	-825	-364	331
3	-800	-452	343
4	-775	-536	355
5	-750	-616	368
6	-700	-766	389
7	-650	-905	411
8	-600	-1035	433
9	-550	-1158	454
10	-500	-1274	474

	Leading side – lower edge		
Point	X-axis (mm)	Y-axis (mm)	Z-axis (mm)
1	-837	-295	290
2	-825	-364	299
3	-800	-452	311
4	-775	-536	323
5	-750	-616	335
6	-700	-766	357
7	-650	-905	379
8	-600	-1035	400
9	-550	-1158	421
10	-500	-1274	442

	Trailing side - upper edge		
Point	X-axis (mm)	Y-axis (mm)	Z-axis (mm)
1	1270	-650	257
2	1250	-700	243
3	1200	-773	222
4	1100	-907	186
5	1000	-1041	149
6	900	-1175	112
7	800	-1308	75
8	700	-1442	38

	Trailing side - lower edge		
Point	X-axis (mm)	Y-axis (mm)	Z-axis (mm)
1	1270	-650	244
2	1250	-700	229
3	1200	-773	209
4	1100	-907	172
5	1000	-1041	135
6	900	-1175	98
7	800	-1308	61
8	700	-1442	24

Table A-3: Coordinate points for hub and shroud side (case – C)

	Hub side – upper edge		
Point	X-axis (mm)	Y-axis (mm)	Z-axis (mm)
1	643	-1519	14
2	600	-1476	30
3	500	-1396	76
4	400	-1336	123
5	300	-1293	172
6	200	-1263	230
7	100	-1246	285
8	0	-1240	333
9	-100	-1246	376
10	-200	-1263	413
11	-300	-1293	443
12	-400	-1336	478
13	-457	-1368	494

	Hub side – lower edge		
Point	X-axis (mm)	Y-axis (mm)	Z-axis (mm)
1	643	-1519	0
2	600	-1476	6
3	500	-1396	24
4	400	-1336	43
5	300	-1293	61
6	200	-1263	82
7	100	-1246	111
8	0	-1240	151
9	-100	-1246	203
10	-200	-1263	267
11	-300	-1293	345
12	-400	-1336	423
13	-457	-1368	462

	Shroud side - upper edge		
Point	X-axis (mm)	Y-axis (mm)	Z-axis (mm)
1	-100	-2	390
2	-200	-10	306
3	-300	-21	303
4	-400	-38	302
5	-500	-60	302
6	-600	-87	304
7	-700	-119	309
8	-750	-140	312
9	-775	-158	314
10	-800	-185	318
11	-825	-229	323
12	0	0	313
13	100	-2	316
14	200	-10	317
15	300	-21	319
16	400	-38	320
17	500	-60	320
18	600	-87	320
19	700	-119	320
20	800	-157	319
21	900	-201	317
22	1000	-251	312
23	1100	-308	306
24	1200	-379	298
25	1250	-447	291
26	1270	-497	287
27	1281	-569	280

	Shroud side - lower edge		
Point	X-axis (mm)	Y-axis (mm)	Z-axis (mm)
1	-100	-2	237
2	-200	-10	239
3	-300	-21	240
4	-400	-38	244
5	-500	-60	247
6	-600	-87	249
7	-700	-119	258
8	-750	-140	267
9	-775	-158	271
10	-800	-185	283
11	-825	-229	295
12	0	0	245
13	100	-2	244
14	200	-10	247
15	300	-21	254
16	400	-38	258
17	500	-60	262
18	600	-87	266
19	700	-119	269
20	800	-157	272
21	900	-201	275
22	1000	-251	276
23	1100	-308	275
24	1200	-379	270
25	1250	-447	262
26	1270	-497	258
27	1281	-569	256

Table A-4: Coordinate points for leading and trailing side (case – C)

	Leading side – upper edge		
Point	X-axis (mm)	Y-axis (mm)	Z-axis (mm)
1	-837	-295	322
2	-825	-364	331
3	-800	-452	343
4	-775	-536	355
5	-750	-616	368
6	-700	-766	389
7	-650	-905	411
8	-600	-1035	433
9	-550	-1158	454
10	-500	-1274	474

	Leading side – lower edge		
Point	X-axis (mm)	Y-axis (mm)	Z-axis (mm)
1	-837	-295	290
2	-825	-364	299
3	-800	-452	311
4	-775	-536	323
5	-750	-616	335
6	-700	-766	357
7	-650	-905	379
8	-600	-1035	400
9	-550	-1158	421
10	-500	-1274	442

	Trailing side - upper edge		
Point	X-axis (mm)	Y-axis (mm)	Z-axis (mm)
1	1270	-650	257
2	1250	-700	243
3	1200	-773	222
4	1100	-907	186
5	1000	-1041	149
6	900	-1175	112
7	800	-1308	75
8	700	-1442	38

	Trailing side - lower edge		
Point	X-axis (mm)	Y-axis (mm)	Z-axis (mm)
1	1270	-650	244
2	1250	-700	229
3	1200	-773	209
4	1100	-907	172
5	1000	-1041	135
6	900	-1175	98
7	800	-1308	61
8	700	-1442	24

Table A-5: Coordinate points for hub and shroud side (case – D)

	Hub side – upper edge		
Point	X-axis (mm)	Y-axis (mm)	Z-axis (mm)
1	657	-1535	41
2	600	-1476	63
3	500	-1396	100
4	400	-1336	137
5	300	-1293	175
6	200	-1263	212
7	100	-1246	254
8	0	-1240	290
9	-100	-1246	321
10	-200	-1263	347
11	-300	-1293	369
12	-400	-1336	391
13	-470	-1376	405

	Hub side – lower edge		
Point	X-axis (mm)	Y-axis (mm)	Z-axis (mm)
1	657	-1535	28
2	600	-1476	32
3	500	-1396	40
4	400	-1336	47
5	300	-1293	55
6	200	-1263	66
7	100	-1246	86
8	0	-1240	116
9	-100	-1246	155
10	-200	-1263	206
11	-300	-1293	268
12	-400	-1336	331
13	-470	-1376	374

	Shroud side - upper edge		
Point	X-axis (mm)	Y-axis (mm)	Z-axis (mm)
1	-100	-2	269
2	-200	-10	266
3	-300	-21	263
4	-400	-38	262
5	-500	-60	263
6	-600	-87	264
7	-700	-119	269
8	-750	-140	272
9	-775	-158	274
10	-800	-185	278
11	-825	-229	283
12	0	0	273
13	100	-2	276
14	200	-10	277
15	300	-21	279
16	400	-38	280
17	500	-60	280
18	600	-87	280
19	700	-119	280
20	800	-157	279
21	900	-201	277
22	1000	-251	272
23	1100	-308	266
24	1200	-379	258
25	1250	-447	251
26	1270	-497	246
27	1281	-569	240

	Shroud side - lower edge		
Point	X-axis (mm)	Y-axis (mm)	Z-axis (mm)
1	-100	-2	197
2	-200	-10	199
3	-300	-21	200
4	-400	-38	204
5	-500	-60	207
6	-600	-87	209
7	-700	-119	218
8	-750	-140	227
9	-775	-158	235
10	-800	-185	243
11	-825	-229	255
12	0	0	200
13	100	-2	204
14	200	-10	207
15	300	-21	214
16	400	-38	218
17	500	-60	222
18	600	-87	226
19	700	-119	229
20	800	-157	232
21	900	-201	235
22	1000	-251	236
23	1100	-308	235
24	1200	-379	230
25	1250	-447	226
26	1270	-497	224
27	1281	-569	224

Table A-6: Coordinate points for leading and trailing side (case – D)

	Leading side – upper edge		
Point	X-axis (mm)	Y-axis (mm)	Z-axis (mm)
1	-837	-288	284
2	-825	-365	293
3	-800	-457	303
4	-775	-544	312
5	-750	-626	322
6	-700	-782	339
7	-650	-926	355
8	-600	-1060	370
9	-550	-1187	384
10	-470	-1376	405

	Leading side – lower edge		
Point	X-axis (mm)	Y-axis (mm)	Z-axis (mm)
1	-837	-288	257
2	-825	-365	265
3	-800	-457	275
4	-775	-544	284
5	-750	-626	293
6	-700	-782	310
7	-650	-926	326
8	-600	-1060	340
9	-550	-1187	354
10	-500	-1376	374

	Trailing side - upper edge		
Point	X-axis (mm)	Y-axis (mm)	Z-axis (mm)
1	1270	-650	223
2	1250	-700	213
3	1200	-775	198
4	1100	-915	169
5	1000	-1055	140
6	900	-1195	111
7	800	-1335	82
8	700	-1475	53

	Trailing side - lower edge		
Point	X-axis (mm)	Y-axis (mm)	Z-axis (mm)
1	1270	-650	208
2	1250	-700	197
3	1200	-775	182
4	1100	-915	154
5	1000	-1055	125
6	900	-1195	97
7	800	-1335	69
8	700	-1475	40

Table A-7: Coordinate points for hub and shroud side (case - E)

	Hub side – upper edge		
Point	X-axis (mm)	Y-axis (mm)	Z-axis (mm)
1	664	-1542	64
2	600	-1476	85
3	500	-1396	119
4	400	-1336	152
5	300	-1293	186
6	200	-1263	219
7	100	-1246	257
8	0	-1240	290
9	-100	-1246	317
10	-200	-1263	340
11	-300	-1293	358
12	-400	-1336	375
13	-476	-1380	389

	Hub side – lower edge		
Point	X-axis (mm)	Y-axis (mm)	Z-axis (mm)
1	664	-1542	51
2	600	-1476	53
3	500	-1396	57
4	400	-1336	62
5	300	-1293	66
6	200	-1263	74
7	100	-1246	91
8	0	-1240	117
9	-100	-1246	153
10	-200	-1263	200
11	-300	-1293	257
12	-400	-1336	315
13	-476	-1380	358

	Shroud side - upper edge		
Point	X-axis (mm)	Y-axis (mm)	Z-axis (mm)
1	-100	-2	269
2	-200	-10	266
3	-300	-21	263
4	-400	-38	262
5	-500	-60	263
6	-600	-87	264
7	-700	-119	269
8	-750	-140	272
9	-775	-158	274
10	-800	-185	278
11	-825	-229	283
12	0	0	273
13	100	-2	276
14	200	-10	277
15	300	-21	279
16	400	-38	280
17	500	-60	280
18	600	-87	280
19	700	-119	280
20	800	-157	279
21	900	-201	277
22	1000	-251	272
23	1100	-308	266
24	1200	-379	258
25	1250	-447	251
26	1270	-497	246
27	1281	-569	240

	Shroud side - lower edge		
Point	X-axis (mm)	Y-axis (mm)	Z-axis (mm)
1	-100	-2	197
2	-200	-10	199
3	-300	-21	200
4	-400	-38	204
5	-500	-60	207
6	-600	-87	209
7	-700	-119	218
8	-750	-140	227
9	-775	-158	235
10	-800	-185	243
11	-825	-229	255
12	0	0	200
13	100	-2	204
14	200	-10	207
15	300	-21	214
16	400	-38	218
17	500	-60	222
18	600	-87	226
19	700	-119	229
20	800	-157	232
21	900	-201	235
22	1000	-251	236
23	1100	-308	235
24	1200	-379	230
25	1250	-447	226
26	1270	-497	224
27	1281	-569	224

Table A-8: Coordinate points for leading and trailing side (case – E)

	Leading side – upper edge		
Point	X-axis (mm)	Y-axis (mm)	Z-axis (mm)
1	-837	-288	284
2	-825	-365	293
3	-800	-457	303
4	-775	-544	312
5	-750	-626	322
6	-700	-782	339
7	-650	-926	355
8	-600	-1060	370
9	-550	-1187	384
10	-470	-1376	405

	Leading side – lower edge		
Point	X-axis (mm)	Y-axis (mm)	Z-axis (mm)
1	-837	-288	257
2	-825	-365	265
3	-800	-457	275
4	-775	-544	284
5	-750	-626	293
6	-700	-782	310
7	-650	-926	326
8	-600	-1060	340
9	-550	-1187	354
10	-470	-1376	374

	Trailing side - upper edge		
Point	X-axis (mm)	Y-axis (mm)	Z-axis (mm)
1	1270	-650	223
2	1250	-700	213
3	1200	-775	198
4	1100	-915	169
5	1000	-1055	140
6	900	-1195	111
7	800	-1335	82
8	700	-1475	53

	Trailing side - lower edge		
Point	X-axis (mm)	Y-axis (mm)	Z-axis (mm)
1	1270	-650	208
2	1250	-700	197
3	1200	-775	182
4	1100	-915	154
5	1000	-1055	125
6	900	-1195	97
7	800	-1335	69
8	700	-1475	40

APPENDIX-B

Table B-1: Result of static analysis on different discharge conditions (case-B)

S.No	Discharge (m3/s)	Total Pressure (Pa)	Von Mises Maximum Stress (MPa)	Maximum Displacement (mm)
1	34.26	102,944	56.3	2.14
2	37.38	103,504	56.6	2.16
3	40.49	104,112	56.9	2.17
4	43.89	104,831	57.3	2.19
5	47.29	105,609	57.8	2.20
6	50.69	106,444	58.2	2.22
7	54.37	107,414	58.7	2.24
8	58.19	108,492	59.3	2.26
9	62.16	109,691	60.0	2.29
10	66.4	111,058	60.7	2.31
11	70.65	112,518	61.5	2.35
12	75.46	114,281	62.5	2.38
13	80.7	116,333	63.6	2.42
14	86.08	118,584	64.9	2.47

Table B-2: Result of static analysis on different discharge conditions (case-C)

S.No	Discharge (m3/s)	Total Pressure (Pa)	Von Mises Maximum Stress (MPa)	Maximum Displacement (mm)
1	34.26	102,944	55.2	2.09
2	37.38	103,504	55.5	2.10
3	40.49	104,112	55.9	2.11
4	43.89	104,831	56.2	2.13
5	47.29	105,609	56.7	2.14
6	50.69	106,444	57.1	2.16
7	54.37	107,414	57.6	2.18
8	58.19	108,492	58.2	2.20
9	62.16	109,691	58.9	2.22
10	66.4	111,058	59.6	2.25
11	70.65	112,518	60.4	2.28
12	75.46	114,281	61.3	2.32
13	80.7	116,333	62.4	2.36
14	86.08	118,584	63.6	2.40

Table B-3: Result of static analysis on different discharge conditions (case-D)

S.No	Discharge (m3/s)	Total Pressure (Pa)	Von Mises Maximum Stress (MPa)	Maximum Displacement (mm)
1	34.26	102,944	55.7	1.97
2	37.38	103,504	56.0	1.98
3	40.49	104,112	56.3	1.99
4	43.89	104,831	56.7	2.01
5	47.29	105,609	57.1	2.02
6	50.69	106,444	57.6	2.04
7	54.37	107,414	58.1	2.06
8	58.19	108,492	58.7	2.08
9	62.16	109,691	59.3	2.10
10	66.4	111,058	60.1	2.13
11	70.65	112,518	60.9	2.16
12	75.46	114,281	61.8	2.19
13	80.7	116,333	62.9	2.23
14	86.08	118,584	64.2	2.27

Table B-4: Result of static analysis on different discharge conditions (case-E)

S.No	Discharge (m3/s)	Total Pressure (Pa)	Von Mises Maximum Stress (MPa)	Maximum Displacement (mm)
1	34.26	102,944	55.3	1.95
2	37.38	103,504	55.6	1.96
3	40.49	104,112	55.9	1.97
4	43.89	104,831	56.3	1.99
5	47.29	105,609	56.7	2.00
6	50.69	106,444	57.2	2.02
7	54.37	107,414	57.7	2.04
8	58.19	108,492	58.3	2.06
9	62.16	109,691	58.9	2.08
10	66.4	111,058	59.6	2.11
11	70.65	112,518	60.4	2.13
12	75.46	114,281	61.4	2.17
13	80.7	116,333	62.5	2.21
14	86.08	118,584	63.7	2.25